AD-A085 747 CORNELL UNIV ITHACA N Y DEPT OF STRUCTURAL ENGINEERING F/G 20/3
NUMERICAL SOLUTIONS FOR COUPLED MAGNETOMECHANICS.(U)
FEB 80 K YUAN, F C MOON, J F ABEL N00014-79-C-0224
UNCLASSIFIED 80-5 NL

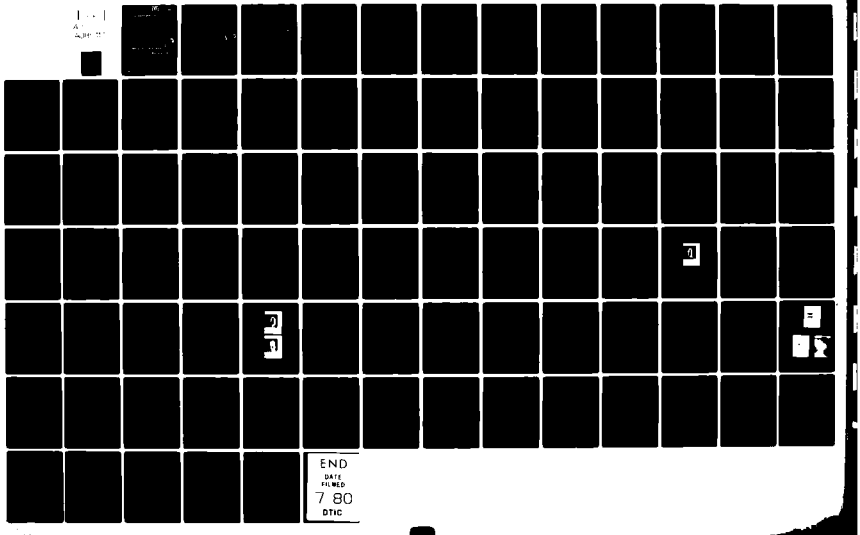

END
DATE FILMED
7 80
DTIC

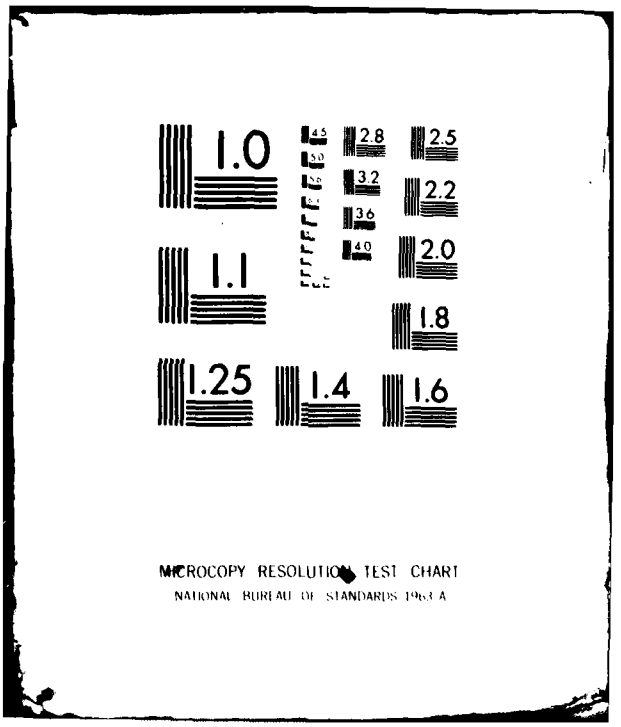
1.0
1.1
1.25
1.4
1.6
1.8
2.0
2.2
2.5
2.8
3.2
3.6
4.0
MICROCOPY RESOLUTION TEST CHART
NATIONAL BUREAU OF STANDARDS 1963 A

LEVEL II

12

Cornell University

Magnetomechanics Research

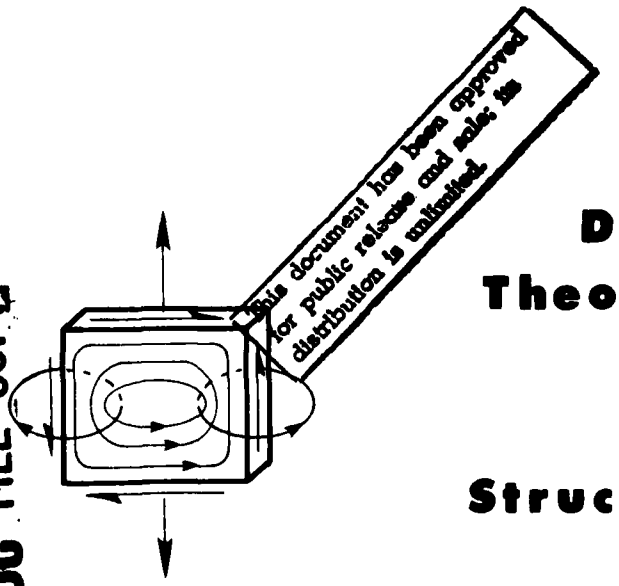

Departments of Theoretical & Applied Mechanics and Structural Engineering

(12)

Interim Technical Report

NUMERICAL SOLUTIONS FOR COUPLED MAGNETOMECHANICS

Kuan-Ya Yuan, Francis C. Moon, and John F. Abel

Department of Structural Engineering Report
Number 80-5

submitted to the
Office of Naval Research
Structural Mechanics Program, Material Sciences Division
ONR Contract No. N00014-79-C-0224

Departments of Structural Engineering
and Theoretical & Applied Mechanics
Cornell University
Ithaca, New York 14853

February 1, 1980

(14) 80-5

SECURITY CLASSIFICATION OF THIS PAGE (When Data Entered)

REPORT DOCUMENTATION PAGE	READ INSTRUCTIONS BEFORE COMPLETING FORM
1. REPORT NUMBER	2. GOVT ACCESSION NO. AD-A085 147 / 3. RECIPIENT'S CATALOG NUMBER (1)
4. TITLE (and Subtitle) (4) NUMERICAL SOLUTIONS FOR COUPLED MAGNETOMECHANICS.	5. TYPE OF REPORT & PERIOD COVERED Interim Technical Report. 1 Feb 79 — 31 Jan 80
	6. PERFORMING ORG. REPORT NUMBER Dept. Struct. Engrg. 80-5
7. AUTHOR(s) (10) Kuan-Ya Yuan, Francis C. Moon, and John F. Abel	8. CONTRACT OR GRANT NUMBER(s) ONR Contract No. N00014-79-C-0224 (15)
9. PERFORMING ORGANIZATION NAME AND ADDRESS Departments of Structural Engineering and Theoretical & Applied Mechanics, Cornell University, Ithaca, NY 14853	10. PROGRAM ELEMENT, PROJECT, TASK AREA & WORK UNIT NUMBERS (12) 87
11. CONTROLLING OFFICE NAME AND ADDRESS Office of Naval Research Resident Representative, Room 323 Federal Bldg., 100 State Street, Rochester, NY 14614	12. REPORT DATE (11) 1 Feb 1980 / 13. NUMBER OF PAGES 81 + vi
14. MONITORING AGENCY NAME & ADDRESS (if different from Controlling Office) Director, Structural Mechanics Programs, Material Science Division, Office of Naval Research, Arlington, VA 22217	15. SECURITY CLASS. (of this report) Unclassified
	15a. DECLASSIFICATION/DOWNGRADING SCHEDULE

16. DISTRIBUTION STATEMENT (of this Report)

No restrictions.

This document has been approved for public release and sale; its distribution is unlimited.

17. DISTRIBUTION STATEMENT (of the abstract entered in Block 20, if different from Report)

18. SUPPLEMENTARY NOTES

19. KEY WORDS (Continue on reverse side if necessary and identify by block number)

Eddy currents, Finite element method, Magnetic forces, Magnetomechanics, Nondestructive testing, Numerical methods.

20. ABSTRACT (Continue on reverse side if necessary and identify by block number)

This technical report describes the accomplishments of the first year of a research project directed toward developing numerical methods for the coupled analysis of forces, currents, and stresses in thin elastic structures exposed to time-dependent magnetic fields. To date research has focused on the response of flat plates to steady state harmonic and pulsed fields. A stream function for the induced eddy currents is used to reduce the three-dimensional electromagnetic problem to an integro-differential equation in two dimensions.

DD FORM 1 JAN 73 1473 403987 Unclassified (over) JC

Finite element codes for one- and two-dimensional flat plates have been developed which can calculate the induced current and magnetic fields, the magnetic pressure distribution, and the temperatures due to Joule heating. These programs have been verified by comparison to experimental results and to known solutions. Application of these programs has indicated the following: (1) the numerical method based on the stream function formulation is successful and appears to hold much greater potential for efficiency than full three-dimensional analysis; (2) for medium to high magnetic Reynolds numbers, the nonlocal effects of the self-field are significant; and (3) the techniques and programs developed should have applications to such problems as electromagnetic nondestructive testing for flaws and cracks in thin sheets of materials and geomagnetic prospecting.

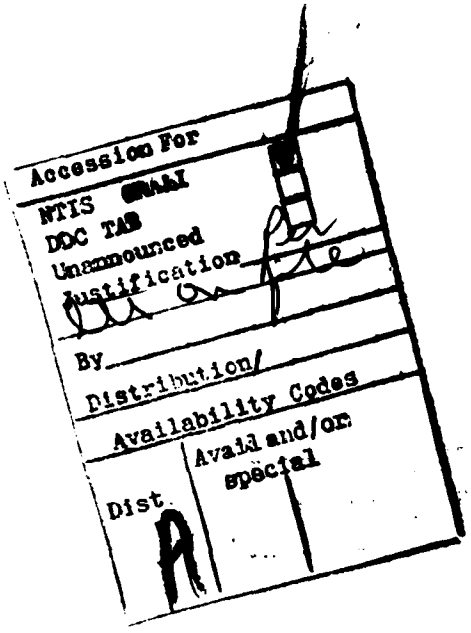

TABLE OF CONTENTS

		Page
	REPORT DOCUMENTATION PAGE	iii
	LIST OF FIGURES	1
I.	INTRODUCTION	3
II.	FORMULATIONS	7
	Review of Basic Theory	7
	Eddy Currents, Pressures and Temperatures by the Stream Function Method	15
	Flat Plate	17
	Cylindrical Shell	18
	Coupled Magnetomechanics	22
III.	ONE-DIMENSIONAL CODE FOR FLAT PLATES	26
	Formulation	26
	Capabilities of the Program ONED	29
	Input	29
	Output	30
IV.	TWO-DIMENSIONAL CODE FOR FLAT PLATES	32
	Formulation	32
	Capabilities of the Program TWOD	34
	Input	34
	Output	35
V.	NUMERICAL RESULTS AND EXPERIMENTAL VERIFICATION	36
	One-Dimensional Analysis	36
	Comparison of FEM and Direct Quadrature for R<<1	38
	Comparison with the Image Method	38
	Nonlocal vs. Local Theory for Eddy Currents	38
	Comparison of FE Calculations with Experimental Measurements	43

Page

FE and FFT Methods for Pulsed Magnetic Fields 50

Effect of Edges on Induced Eddy Currents 52

Pressure Distributions Due to Tilted Induction Coils 52

Effect of Reduced Matrix Band on Nonlocal Solutions 52

Two-Dimensional Analysis 57

Nondestructive Testing (NDT) Application 59

VI. CONCLUSIONS 65

REFERENCES 67

APPENDICES 69

A. Description of Experimental Apparatus 69

B. Personnel Engaged in the Research 72

C. Communication of Technical Results 73

DISTRIBUTION LIST 74

LIST OF FIGURES

		Page
II-1	A Schematic of One Form of Magnetothermomechanical Coupling	8
II-2	Eddy Current Flow in Thin Conductors Showing External and Induced Magnetic Fields	13
II-3	Notation, Coordinates, and Sign Convention for Cylindrical Shell	19
II-4	A Possible Algorithm for Large-Deformation, Coupled Magnetomechanics	24
III-1	Notation, Sign Conventions, and Shape Functions for One-Dimensional Flat-Plate Problems	27
V-1	Induced Currents in a Long Rectangular Plate	37
V-2	Comparison of FEM and Direct Quadrature Solutions for Low R for a Pair of Current Filaments Centered Above a Long Conducting Plate (R = 0.01)	39
V-3	The Image Method for High R	40
V-4	Comparison of FEM and Image Method Solutions for High R for a Pair of Current Filaments Centered Above a Long Conducting Plate (R = 5)	41
V-5	Comparison of Nonlocal and Local Solutions for a Pair of Current Filaments Centered Above a Long Conducting Plate (R = 0.1)	42
V-6	Method of Detecting Eddy Current Flow Patterns in Thin Structures	45
V-7	Photograph of an Infrared Thermogram for Currents in a Plate as Induced by a Pulsed Rectangular Coil	46
V-8	Comparison of FE Solution and Measured Temperatures for a Pair of Current Filaments Centered Above a Long Conducting Plate (R = 0.071)	47
V-9	Comparison of FE Solution and Measured Temperatures for a Pair of Current Filaments Nearer One Edge of a Long Conducting Plate (R = 0.074)	48
V-10	Transient Exciting and Induced Currents as Functions of Time	49

		Page
V-11	Spectrum for Current at x = -0.62A for Local and Nonlocal Solutions	51
V-12	Photographs Showing Effects of Edges on Induced Eddy Currents	53
V-13	Calculated Edge Effects for Uniform Induction Field	54
V-14	Magnetic Pressures Due to a Tilted Pair of Current Filaments Centered Above a Long Conducting Plate (R = 0.07, tilt = 10°)	55
V-15	Magnetic Pressures Due to a Tilted Pair of Current Filaments Nearer One Edge of a Long Conducting Plate (R = 0.07, tilt = 10°)	56
V-16	Effect of Reduced Matrix Band on Nonlocal Solutions for a Pair of Current Filaments Centered Above a Long Conducting Plate (R = 0.071)	58
V-17	Stream Function Contours for a Long Rectangular Plate Excited by a Harmonic Uniform Field (R = 0.0012)	60
V-18	Comparison of One- and Two-Dimensional Solutions of Currents Induced Across the Middle of a Long Rectangular Plate by a Harmonic Uniform Field (R = 0.03)	61
V-19	Infrared Thermogram Showing Hot Spots Due to Eddy Current Flow	62
V-20	Stream Function Contours for a Notched Plate Excited by a Harmonic Uniform Field (Notchwidth = 2h, R = 0.001)	63
V-21	Isotherms for a Notched Plate Excited by a Harmonic Uniform Field (Notchwidth = 2h, R = 0.001)	64

I. INTRODUCTION

There is an increasing number of design problems which involve the coupling of magnetic fields, induced currents and mechanical behavior. Moreover, many of these problems also involve thermal effects which may or may not be coupled with the magnetomechanical behavior. Among the types of machinery and devices for which such coupled behavior is significant are superconducting motors and generators [1] fusion reactors [2], magnetic levitation transport systems [2], transmission lines, magnetomotive tools [3], [4], inductive storage units, MHD devices [2], and various other electromagnetic devices and switches [5]. Other objects subject to these phenomena are structures or devices called on to withstand lightning or electrical shorting in high voltage switches [5]. A review of many of these coupled problems in magneto-solid mechanics has been presented by Moon [11].

The computational problems involved in analysis of the coupled behavior of such structures are formidable. Therefore, prevailing practice has been to undertake separate analyses of the magnetic, thermal and mechanical effects. A magnetic field and induced current analysis is first undertaken to predict the magnetic forces on the assumed rigid structure. Temperature fields are next predicted. As a final step, analysis for the uncoupled mechanical response is performed.

This uncoupled approach may be inadequate in several regards. First, the deformation of the structure will alter the induced currents and the concommitant forces, and this effect will lead to altered structural response and may produce structural instabilities. (For example, such magnetomechanical instabilities have been found in structures for proposed fusion reactors [6], [7]). Second, in dynamic problems the eddy currents may give rise to thermoelastic effects. Finally, in superconducting problems, the vast thermal

differences and gradients will have a pronounced effect not only on the magnetic behavior but also on the material nonlinearities entering the mechanical behavior.

The goal of ongoing research at Cornell is to develop numerical methods for the coupled analysis of forces, currents, and stresses in thin elastic structures exposed to time-dependent magnetic fields. In particular the project is directed toward time dependent magnetic forces and motions of elastic plates and shells. Both applied mathematical analysis and finite element numerical computer techniques are being used. Although some initial attempts have already been made by others (Oden and Kelley [8]; Miya et al. [9]; Becker and Pillsbury [10]), many fundamental difficulties remain to be overcome if practical analysis tools are eventually to result. Verification of the newly developed computer codes is carried out by direct comparison of the calculated results with experimental data and is carried out at each stage of the development. The experiments employ a new infrared scanning technique to visualize the induced eddy current patterns in the structures. This technical report is an account of the first year's accomplishments in this effort.

Coupled magnetomechanical problems are unique in that the electromagnetic field equations apply both inside and outside the structural material. Thus most techniques for calculating stresses due to electromagnetic fields require a three dimensional treatment even if the structure is one or two-dimensional such as a beam, plate, or shell. In this research a stream function for the induced current in the conducting structure has been used which reduces the magnetics problem to a two-dimensional one and allows one to use the same set of finite elements for both the magnetic and elastic deformation fields. The use of a current potential or stream function is similar to vortex

mechanics in fluid mechanics, and results in an integro-differential equation for the induced currents in the structure. Once these currents are calculated, the magnetic forces, stresses, and motions of the structure can be found. To solve the integro-differential equation, a finite element Galerkin scheme has been developed which leads to an algebraic set of equations for the induced currents. The resulting global matrix is complex, nonsymmetric, and fully populated. The usual limited connectivity (banded matrix) finite element representation is lost in contrast to conventional structural finite element problems.

To date, the research has focused on the response of flat plates to steady state harmonic and pulsed magnetic fields. A finite element code for one-dimensional magnetic field problems has been successfully developed which can calculate the induced current and magnetic field in the plate, the magnetic pressure distribution on the plate, and the induced temperature distribution due to Joule heating in the plate. The computer code has been compared directly with experimental results. Comparison of calculated induced temperature fields with infrared scanning measurements show the difference to be within observational error.

A two-dimensional computer code for the induced currents, magnetic field and temperature in a conducting plate has also been written. The flow of eddy currents around a crack in a plate is one problem investigated with this program. This type of analysis has application to the development of non-destructive testing techniques.

In the next chapter, the formulations of the problem are summarized. This summary includes the basic theory of coupled magnetomechanics, the stream-function method for eddy currents in flat plates and cylindrical shells, and the coupled magnetomechanic formulation for flat plates. Chapters III and IV

contain, respectively, descriptions of the one- and two-dimensional computer programs for eddy currents in flat plates. Numerical results and experimental verification for both programs are presented in Chapter V. Finally, conclusions based on developments to date are presented in Chapter VI.

II. FORMULATIONS

In this chapter, the basic theory of magnetothermomechanics is briefly reviewed. The formulation of the eddy currents by the stream-function method adopted for use in this research for flat plates and cylindrical shells is next presented. Finally, the coupled magnetomechanical formulation for flat plates is summarized.

Review of Basic Theory

Magnetothermomechanics encompasses a rather complicated three-field problem. The coupling of the three fields is shown schematically in Figure II-1 and occurs through the field equations, constitutive equations, and boundary conditions. A number of formulations of the governing equations and boundary conditions for various physical specializations have been presented [11], [12]. For the descriptive purposes of this report, only a single version corresponding to Figure II-1 is presented here.

When a deformable electric conductor is placed in an electromagnetic field $\underset{\sim}{B}$, electric currents flow in the solid and electric and magnetic polarization of the material may be induced. In this study the electric polarization is not considered. The electric currents $\underset{\sim}{J}$ (sometimes called eddy currents) and magnetization $\underset{\sim}{M}$, can then interact with the magnetic field to produce a body force distribution on the solid [13]. Thus to determine the stresses and concommitant deformation of the structure, the distribution of electric currents, magnetic field, and magnetization in the body must be determined. In this research only nonferromagnetic materials ($\underset{\sim}{M} = 0$) such as aluminum or copper have been treated to date.

In addition to magnetic forces, the flow of current produces heating in the solid proportional to $\underset{\sim}{J} \cdot \underset{\sim}{J}$ called Joule heating. If the currents

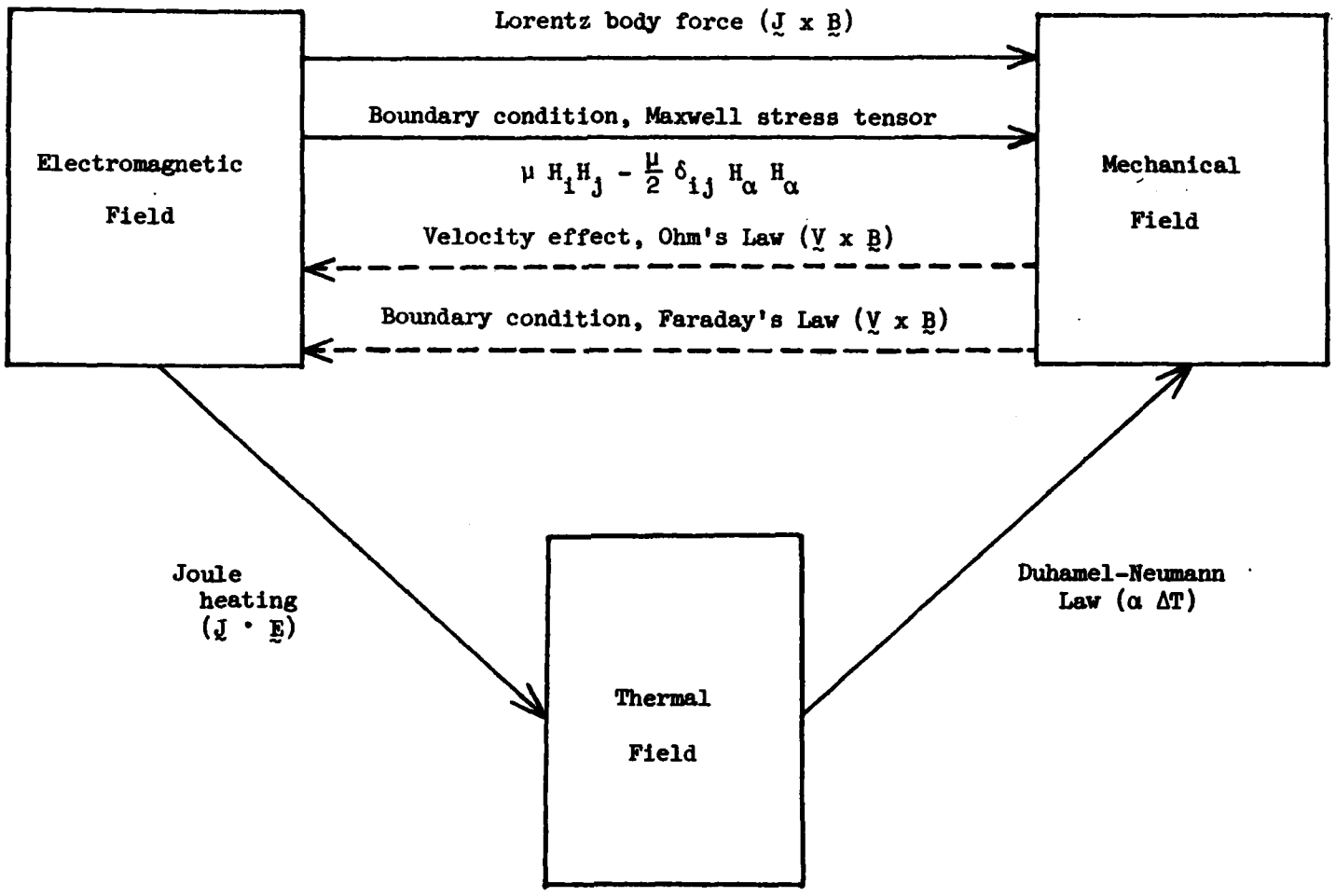

Figure II-1. A Schematic of One Form of Magnetothermomechanical Coupling ($\underset{\sim}{E}$ = electric field, $\underset{\sim}{J}$ = electric current, $\underset{\sim}{B}$ = magnetic flux, $\underset{\sim}{V}$ = velocity field, μ = magnetic permeability, α = coefficient of thermal expansion, ΔT = change in temperature from reference temperature, $\underset{\sim}{H}$ = magnetic intensity.)

are confined to one region of the structure then differential heating can occur and thermoelastic stresses can result.

The following equations and boundary conditions apply to the problem of dynamic thermoelasticity coupled to the quasistatic electromagnetics of a medium. The medium is assumed to be well conducting, non-polarizable and non-magnetizable. The influence of strain rate on temperature distribution is assumed to be small as is the effect of temperature on material properties. All configurations are referred to a Cartesian system (x_1, x_2, x_3) fixed in space. The assumption of quasistatic electromagnetics in association with dynamic mechanical behavior is justified by the fact that the frequencies of mechanical vibrations and waves are generally much smaller than those of electromagnetic waves of the same wave length.

The quasistatic magnetic field equations for this case are obtained from the Maxwell equations and are [13],

$$\underset{\sim}{\nabla} \times \underset{\sim}{E} = -\partial \underset{\sim}{B}/\partial t \qquad \text{(II-1a)}$$

$$\underset{\sim}{\nabla} \cdot \underset{\sim}{B} = 0 \qquad \text{(II-1b)}$$

$$\underset{\sim}{\nabla} \times \underset{\sim}{H} = \underset{\sim}{J} \qquad \text{(II-1c)}$$

in which $\underset{\sim}{E}$ is the electric field density, $\underset{\sim}{B}$ is the magnetic flux density, $\underset{\sim}{H}$ is the magnetic intensity, and $\underset{\sim}{J}$ is the electric current density. The electromagnetic constitutive equations for a linear, isotropic, homogeneous, resistive, nonferromagnetic* material are

$$\underset{\sim}{B} = \mu_o \underset{\sim}{H} \qquad \text{(II-2a)}$$

$$\underset{\sim}{J} = \sigma[\underset{\sim}{E} + \underset{\sim}{V} \times \underset{\sim}{B}] \qquad \text{(II-2b)}$$

*For linear ferromagnetic material one replaces μ_o by $\mu_o\mu_r$, $\mu_r > 1$.

in which μ_o is the magnetic permeability of vacuum, σ is the electric conductivity and $\underset{\sim}{V}$ is the velocity field. For a zero resistive or superconducting material, Ohm's law (II-2b) is replaced by an equation of the form

$$\underset{\sim}{E} = \alpha \dot{\underset{\sim}{J}}$$

The electromagnetic boundary conditions are

$$\underset{\sim}{n} \times \left[\underset{\sim}{E} + \underset{\sim}{V} \times \underset{\sim}{B} \right] = 0 \qquad \text{(II-3a)}$$

$$\underset{\sim}{n} \times \left[\!\left[H \right]\!\right] = 0 \qquad \text{(II-3b)}$$

$$\underset{\sim}{n} \times \left[\!\left[B \right]\!\right] = 0 \qquad \text{(II-3c)}$$

in which $\underset{\sim}{n}$ is a unit normal vector to the boundary, and $\left[\!\left[\underset{\sim}{\Psi} \right]\!\right]$ denotes the jump of the quantity $\underset{\sim}{\Psi}$ across the interface.

The mechanical field equations are the equilibrium equations

$$\rho \frac{\partial^2 u_i}{\partial t^2} = \frac{\partial \tau_{ij}}{\partial x_j} + F_i + (\underset{\sim}{J} \times \underset{\sim}{B})_i \qquad \text{(II-4)}$$

in which $\underset{\sim}{u}$ is the displacement field, τ_{ij} is the stress tensor, $\underset{\sim}{F}$ is the mechanical body force intensity, ρ is the mass density. Equation II-4 includes magnetomechanical coupling* through the Lorentz body force term $(\underset{\sim}{J} \times \underset{\sim}{B})$. The mechanical constitute equations for a linear, isotropic, nonferromagnetic material is given by the Duhamel-Neumann law.

$$\tau_{ij} = 2Ge_{ij} + [\lambda e_{\alpha\alpha} - \beta (T - T_o)] \delta_{ij} \qquad \text{(II-5)}$$

---

*For ferromagnetic bodies an additional force must be added.

in which G and λ are the Lamé parameters, e_{ij} in the strain tensor, T is the temperature, T_o is the initial uniform reference temperature, $\beta = (3d + 2G)\alpha$, and α is the coefficient of thermal expansion. Finally, the mechanical boundary conditions are

$$\tau_{ij} n_j = \bar{T}_i + \left[\mu H_i H_j - \frac{\mu}{2} H_x H_x \delta_{ij}\right] n_j \quad \text{on } S_\tau \tag{II-6a}$$

$$u_i = \bar{u}_i \quad \text{on } S_u \tag{II-6b}$$

in which $S = S_\tau + S_u$, and $\bar{T}_i$ and $\bar{u}_i$ are specified surface tractions and surface displacements.

For the third field, the temperature, the field equations are

$$\rho C_v \frac{\partial T}{\partial t} - K \frac{\partial^2 T}{\partial x_i \partial x_i} = \underset{\sim}{J} \cdot \underset{\sim}{E} \tag{II-7}$$

in which C_v is the specific heat, and K is the thermal conductivity. The Joule heating term, $\underset{\sim}{J} \cdot \underset{\sim}{E}$, provides magnetothermal coupling. The strain rate coupling term has been dropped in (II-7). In the absence of heat input across boundaries and if radiation can be neglected the thermal boundary conditions are

$$T = \bar{T} \quad \text{on S.} \tag{II-8a}$$

$$\underset{\sim}{K_n} \cdot \nabla T = 0 \quad \text{on } S_2 \tag{II-8b}$$

in which $S = S_1 + S_2$, and $\bar{T}$ is the specified surface temperatures.

Equations II-1 through II-8 constitute an example of a coupled problem of the form shown schematically on Fig. II-1. A practice frequently followed is an uncoupled approach in which first the electromagnetic problem is solved for "rigid" conductors, second the temperature distribution due to Joule heating

is ascertained, and finally the mechanical problem for the conductors is considered driven by the known temperatures and Lorentz forces. This simplified problem is obtained in Figure II-1 by omitting the dashed coupling lines from the schematic.

For dynamic magnetic fields even the uncoupled electromagnetic problem is difficult to solve since the induced currents in the conductor are unknown. When an external magnetic field $\underset{\sim}{B}^0$ induces eddy currents in a conductor these currents generate their own self magnetic field $\underset{\sim}{B}^1$ (see Figure II-2) which in turn affects the eddy current problem. Several problems of this nature have been solved using finite element methods ([14] - [17]). These approaches however use a finite element discretization both inside and outside the conductor which makes the extension of these numerical schemes to coupled mechanical problems difficult.

Two different solution approaches to the eddy current problem have been undertaken. The first, or <u>local approach</u>, seeks to solve the differential field equations and satisfy all the boundary and initial conditions directly. The domain of the solution is the entire space in which the fields act and includes the current-source conductors, the induced-current conductors, and the surrounding space (theoretically out to an infinite distance). The second, or <u>nonlocal approach</u>, uses integral restatements of the formulation such that only the bodies of the conductors themselves need be considered in the problem. Thus this approach avoids treatment of free space extending to infinity and may be easier to extend to coupled magneto-mechanical problems.

Briefly, the <u>local</u> approach for the uncoupled problem of Eqs. II-1 through II-8 above is most conveniently expressed in terms of the magnetic vector potential $\underset{\sim}{A}$, defined by

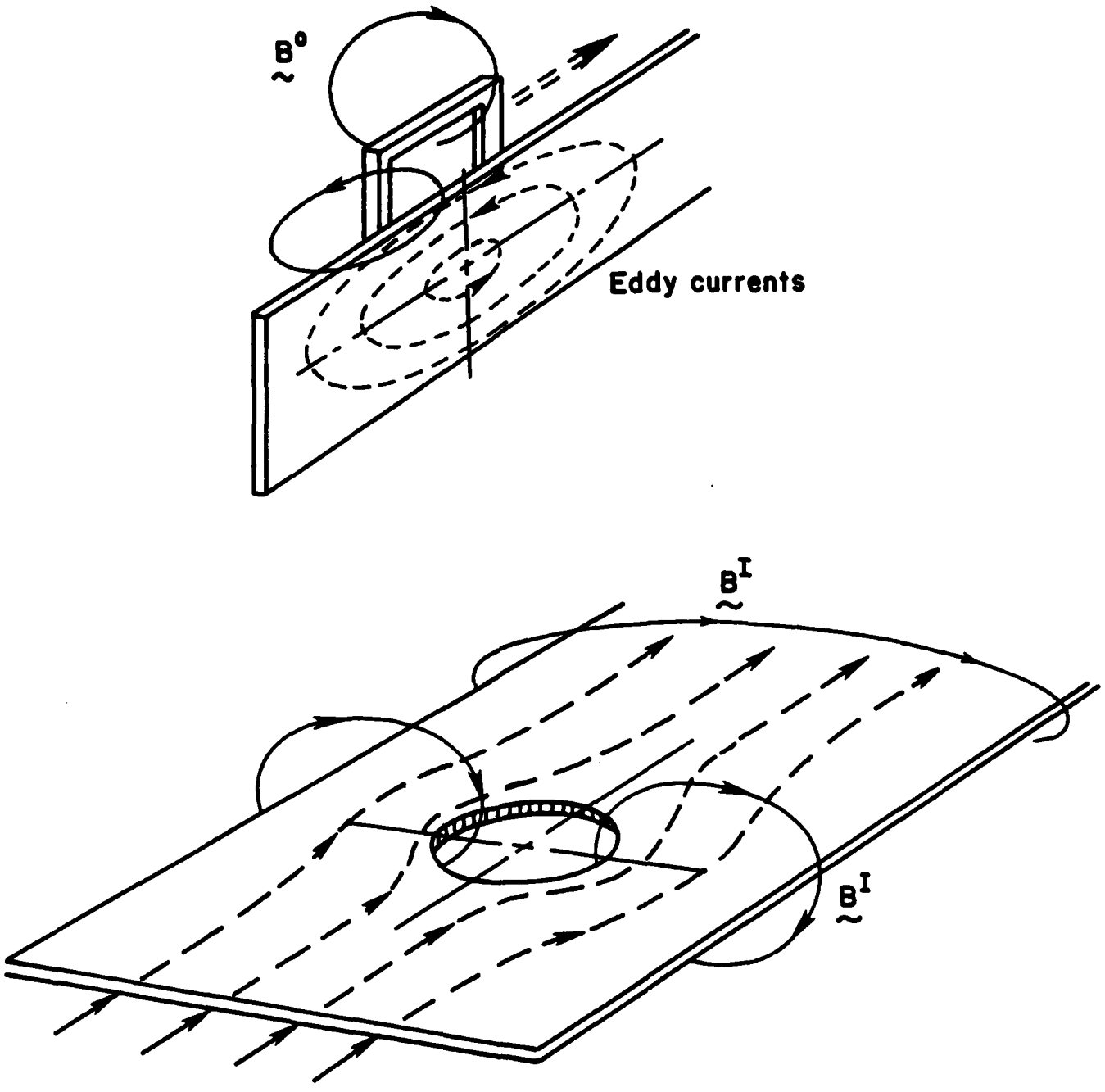

Figure II-2. Eddy Current Flow in Thin Conductors Showing External and Induced Magnetic Fields.

$$\underset{\sim}{B} = \underset{\sim}{\nabla} \times \underset{\sim}{A} \quad (\text{since } \nabla \cdot \underset{\sim}{B} = 0) \tag{II-9}$$

The governing equations for the potential $\underset{\sim}{A}$ in the conductor become

$$\sigma \dot{\underset{\sim}{A}} + \frac{1}{\mu} \underset{\sim}{\nabla} \times \underset{\sim}{\nabla} \times \underset{\sim}{A} - \sigma \dot{\underset{\sim}{u}} \times \underset{\sim}{\nabla} \times \underset{\sim}{A} = \underset{\sim}{J}_o \tag{II-10}$$

in which $\underset{\sim}{J}_o$ is the initial current density carried by the conductor. Outside the conductors $\sigma = \dot{\underset{\sim}{u}} = 0$ and $\underset{\sim}{A}$ must satisfy

$$\nabla \times \nabla \times \underset{\sim}{A} = 0$$

for non-electromagnetic wave problems. Thus the solution for $\underset{\sim}{A}$ must be pieced together for regions outside and inside the conductors using appropriate boundary conditions. It is difficult to couple a structural finite element scheme for the deformation of the conductors using this local formulation. A Galerkin finite element formulation can be used for this form of the problem ([14] - [17]), but details will not be repeated here.

Alternatively, a <u>nonlocal formulation</u> for the eddy current problem may be constructed by the integral equation method. Here the vector potential is separated into two independent parts, $\underset{\sim}{A}^o$ and $\underset{\sim}{A}^I$:

$$\underset{\sim}{A} = \underset{\sim}{A}^o + \underset{\sim}{A}^I \tag{II-11}$$

corresponding to the driving and induced fields, respectively. Ohm's law for the rigid, induced-current conductor may be written as

$$\underset{\sim}{J}^I = \sigma \underset{\sim}{E}^I = -\sigma \frac{\partial}{\partial t} \underset{\sim}{A}^o - \sigma \frac{\partial}{\partial t} A^o - \sigma \frac{\partial}{\partial t} \underset{\sim}{A}^I \tag{II-12}$$

where $\underset{\sim}{J}^o$ has been assumed to be zero, i.e., no external voltage is applied to the induced-current conductor. Within the conductor, the external field satisfies $\underset{\sim}{\nabla} \times \underset{\sim}{H}^o = 0$; therefore, A^o is harmonic, i.e., $\nabla^2 \underset{\sim}{A}^o = 0$, while the induced field satisfies the vector Poisson equation

$$\nabla^2 \underset{\sim}{A}^I = -\mu \underset{\sim}{J}^I \tag{II-13}$$

because $\underset{\sim}{\nabla} \times \underset{\sim}{H}^I = \underset{\sim}{J}^I$. If retardation is neglected due to sufficiently slow variation of all electromagnetic quantities with time, the solution of Eq. (II-13) for $\underset{\sim}{A}^I$ is

$$\underset{\sim}{A}^I = \frac{\mu}{4\pi} \int_V \frac{\underset{\sim}{J}^I (\underset{\sim}{r}')}{|\underset{\sim}{x} - \underset{\sim}{x}'|} \, d(\text{Vol}') \tag{II-14}$$

which gives an integral equation in terms of $\underset{\sim}{J}^I$

$$\underset{\sim}{J}^I + \frac{\sigma\mu}{4\pi} \int_V \frac{1}{|\underset{\sim}{r} - \underset{\sim}{r}'|} \frac{\partial}{\partial t} \underset{\sim}{J}^I (\underset{\sim}{r}') \, d(\text{Vol}') = -\sigma \frac{\partial}{\partial t} \underset{\sim}{A}^\circ \tag{II-15}$$

or in terms of $\underset{\sim}{A}^I$

$$\underset{\sim}{A}^I + \frac{\sigma\mu}{4\pi} \int_V \frac{1}{|\underset{\sim}{r} - \underset{\sim}{r}'|} \frac{\partial}{\partial t} A^I (r') \, d(\text{Vol}') = \underset{\sim}{A}^\circ \tag{II-16}$$

A finite-element-like treatment of this formulation of the eddy current problem has been presented by Sylvester et al. [18].

Eddy Currents, Pressures and Temperatures by the Stream Function Method

When conductors are thin-sheet structures such as plates or shells which are used in many practical configurations, a different nonlocal approach for the eddy current problem suggested by Moon [11] can be of greater utility than the integral equation method. This involves the introduction of a stream function for the current. If the current is of relatively low frequency, the induced current distribution can be assumed to be uniform through the thickness, and the current density is denoted by $\underset{\sim}{I} = h\underset{\sim}{J}$ where h is the thickness of the sheet. Let (α,β) be a two-dimensional orthogonal coordinate system on the mid-surface of the sheet conductor structure, and let (x,y,z) be a Cartesian

coordinate system, so that

$$x = x(\alpha,\beta), \quad y = y(\alpha,\beta), \quad z = z(\alpha,\beta) \tag{II-17}$$

The infinitesimal line element on the surface is given by

$$ds^2 = f^2 d\alpha^2 + g^2 d\beta^2 \tag{II-18}$$

in which

$$f^2 = \left(\frac{\partial x}{\partial \alpha}\right)^2 + \left(\frac{\partial y}{\partial \alpha}\right)^2 + \left(\frac{\partial z}{\partial \alpha}\right)^2$$

$$g^2 = \left(\frac{\partial x}{\partial \beta}\right)^2 + \left(\frac{\partial y}{\partial \beta}\right)^2 + \left(\frac{\partial z}{\partial \beta}\right)^2 \tag{II-19}$$

The orthogonality of (α,β) coordinate system requires that

$$\left(\frac{\partial x}{\partial \alpha}\right)\left(\frac{\partial x}{\partial \beta}\right) + \left(\frac{\partial y}{\partial \alpha}\right)\left(\frac{\partial y}{\partial \beta}\right) + \left(\frac{\partial z}{\partial \alpha}\right)\left(\frac{\partial z}{\partial \beta}\right) = 0 \tag{II-20}$$

Let $\underset{\sim}{e}_\alpha$ and $\underset{\sim}{e}_\beta$ be unit tangent vector along α = constant and β = constant, respectively.

$$\underset{\sim}{e}_\alpha = \begin{pmatrix} \frac{1}{f}\frac{\partial x}{\partial \alpha} \\ \frac{1}{f}\frac{\partial y}{\partial \alpha} \\ \frac{1}{f}\frac{\partial z}{\partial \alpha} \end{pmatrix}, \quad \underset{\sim}{e}_\beta = \begin{pmatrix} \frac{1}{g}\frac{\partial x}{\partial \beta} \\ \frac{1}{g}\frac{\partial y}{\partial \beta} \\ \frac{1}{g}\frac{\partial z}{\partial \beta} \end{pmatrix} \tag{II-21}$$

The current density on the surface can be written in the form

$$\underset{\sim}{I} = I^\alpha(\alpha,\beta)\,\underset{\sim}{e}_\alpha + I^\beta(\alpha,\beta)\,\underset{\sim}{e}_\beta \tag{II-22}$$

The continuity of $\underset{\sim}{I}$ requires that

$$\operatorname{div} \underset{\sim}{I} = \frac{1}{f\cdot g}\left[\frac{\partial}{\partial \alpha}(gI^\alpha) + \frac{\partial}{\partial \beta}(fI^\beta)\right] = 0 \tag{II-23}$$

This suggests the use of a stream function Ψ for the current

This function, when defined as

$$I^\alpha = \frac{1}{g}\frac{\partial \psi}{\partial \beta}, \quad I^\beta = -\frac{1}{f}\frac{\partial \psi}{\partial \alpha} \tag{II-24}$$

identically satisfies the continuity condition. The current flows along lines of Ψ = constant. The time-varying magnetic field is the sum of the external field, $\underset{\sim}{B}^{o}$, and the induced field, $\underset{\sim}{B}^{I}$. Therefore, from Faraday's law, Equation II-1(a), curl $\underset{\sim}{E} = -\frac{\partial}{\partial t}\underset{\sim}{B}$, one may write a governing equation for the determination of Ψ:

$$\text{curl} \cdot \text{curl}\,(\psi \underset{\sim}{n}) = \sigma h \frac{\partial}{\partial t}(\underset{\sim}{B}^{o} + \underset{\sim}{B}^{I}) \tag{II-25}$$

Only the normal ($\underset{\sim}{n}$) component of the vector equation will be used because the in-plane current is of primary interest. The induced field may be obtained from the Biot-Savart law. The specific derivations are given below for flat plates and thin cylindrical shells. Once the relationship between the induced field and the stream function is obtained, Ψ may be determined from Eq. (II-25). The current can be recovered from Eq. (II-24), and magnetic pressure and temperature then obtained for the calculated current.

Flat plate. The derivation for the case of a flat plate has been given by Moon [11]. The details are not repeated here; only the essential relationships are recapitulated.

If the mid-plane of the plate is chosen as the xy plane, $\alpha = x$, $\beta = y$, and one obtains

$$\underset{\sim}{I} = \nabla \times (\psi \underset{\sim}{n}) = -\underset{\sim}{n} \times \nabla\psi \tag{II-26}$$

and

$$\nabla^2 \psi = \sigma h \frac{\partial}{\partial t}(B_z^{o} + B_z^{I}) \tag{II-27}$$

For the determination of B_z^{I}, the current stream function Ψ is assumed to be defined throughout three-dimensional space, and constant across the

sheet thickness. Application of the Biot-Savart law and the divergence theorem yields B_z^I for the midplane of the plate ($z = 0$):

$$B^I(x,y,o) = \frac{\mu}{h}\psi - \frac{\mu}{4\pi}\int_{\text{area}} \frac{\psi(x',y')\ d(\text{area}')}{[(x-x')^2 + (y-y')^2 + (\frac{h}{2})^2]^{3/2}} \qquad \text{(II-28)}$$

Ψ has been set to zero on the boundary of the plate in the above derivation. When the plate is multiply connected, different constant values of Ψ will be assigned on each interior boundary. These boundary conditions, together with the known B_z^o and Eq. (II-28), are then used in (II-27) for the determination of the stream function Ψ. Once Ψ is determined, the current, pressure, and temperature may be calculated from (II-26) and the following two equations

$$\underset{\sim}{P} = \underset{\sim}{I} \times (\underset{\sim}{B}^o + \underset{\sim}{B}^I) \qquad \text{(II-29)}$$

$$T = \frac{1}{\sigma\rho C_v h^2}\int_o^t (\underset{\sim}{I}\cdot\underset{\sim}{I})dt \qquad \text{(II-30)}$$

in which $\underset{\sim}{P}$ is the pressure, T the temperature rise, ρ the density, and C_v the specific heat of the conductor.

Cylindrical shell. The stream function method has been extended to the geometry of a cylindrical shell. In this case the coordinate system is chosen as shown in Fig. II-3. For a fixed radius $\rho = a$, one has $\alpha = \phi$, $\beta = z$. The stream function Ψ may be introduced such that

$$\underset{\sim}{I} = \nabla \times (\psi \underset{\sim}{e}_\rho) = \frac{\partial\psi}{\partial z}\underset{\sim}{e}_\phi - \frac{1}{\rho}\frac{\partial\psi}{\partial\phi}\underset{\sim}{e}_z \qquad \text{(II-31)}$$

i.e.

$$I_\phi = \frac{\partial\psi}{\partial z}\ ,\ I_z = -\frac{1}{\rho}\frac{\partial\psi}{\partial\phi} \qquad \text{(II-32)}$$

The normal component of (II-25) in this case reads

$$\frac{1}{\rho^2}\frac{\partial^2\psi}{\partial\phi^2} + \frac{\partial^2\psi}{\partial z^2} = \sigma h \frac{\partial}{\partial t}(B_\rho^o + B_\rho^I) \qquad \text{(II-33)}$$

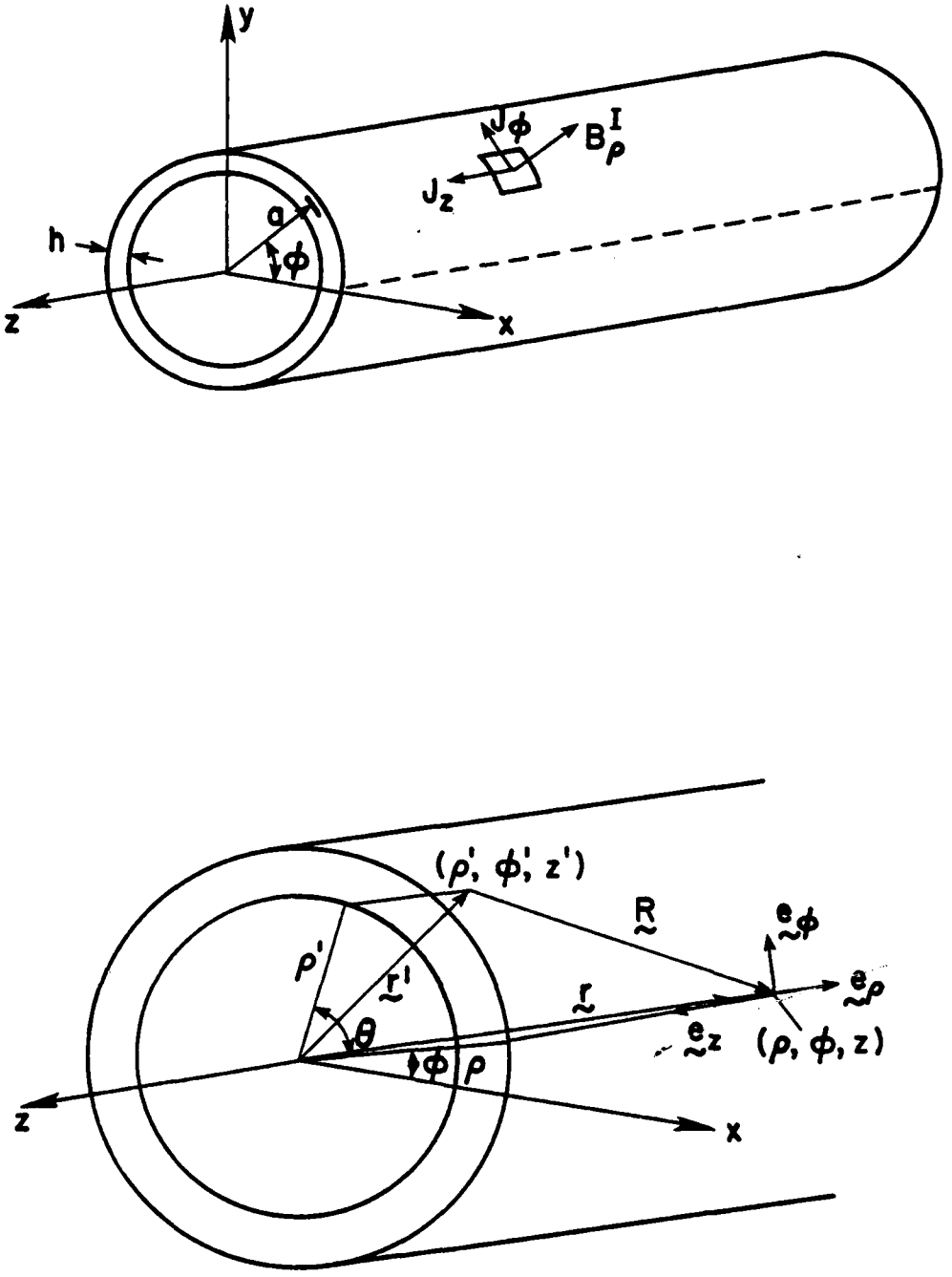

Figure II-3. Notation, Coordinates, and Sign Convention for Cylindrical Shell.

To calculate B_ρ^I one starts from the Biot-Savart law

$$\underset{\sim}{B}^I(\underset{\sim}{r}) = \frac{\mu}{4\pi h} \int_{\text{volume}} \frac{\underset{\sim}{I}(\underset{\sim}{r}') \times (\underset{\sim}{r} - \underset{\sim}{r}')}{|\underset{\sim}{r} - \underset{\sim}{r}'|^3} \, d(\text{Vol.}') \tag{II-34}$$

Let

$$\underset{\sim}{R} = \underset{\sim}{r} - \underset{\sim}{r}', \qquad \theta = \phi - \phi' \tag{II-35}$$

then

$$\underset{\sim}{R} = (\rho\cos\theta - \rho')\, \underset{\sim}{e}_{\rho'} + \rho\sin\theta\, \underset{\sim}{e}_{\theta'} + (z - z')\, \underset{\sim}{e}_{z'} \tag{II-36}$$

Using Eq. (II-32) and the relationship

$$\nabla_1 \frac{1}{|\underset{\sim}{R}|} = \frac{\underset{\sim}{R}}{|\underset{\sim}{R}|^3} \tag{II-37}$$

one has

$$B_\rho^I(\underset{\sim}{r}) = \frac{\mu}{4\pi h} \int_{\text{vol.}} \left[\left(\frac{\partial\psi}{\partial z'}\right)\left(\frac{\partial}{\partial z'} \frac{1}{|\underset{\sim}{R}|}\right) + \left(\frac{1}{\rho'} \frac{\partial\psi}{\partial\phi'}\right)\left(\frac{1}{\rho'} \frac{\partial}{\partial\phi'} \frac{1}{|\underset{\sim}{R}|}\right)\right] d(\text{vol.}') \tag{II-38}$$

The integrand can be written in the form

$$\nabla_1\psi\, \nabla_1 \frac{1}{|\underset{\sim}{R}|} - \frac{\partial\psi}{\partial\rho'} \left(\frac{\partial}{\partial\rho'} \frac{1}{|\underset{\sim}{R}|}\right) \tag{II-39}$$

The second term vanishes because $\frac{\partial\Psi}{\partial\rho'} = 0$. Using an identity to replace the first term, one obtains the expression for B_ρ^I as

$$B_\rho^I(\underset{\sim}{r}) = \frac{\mu}{4\pi h} \int_{\text{vol.}} \left\{\nabla_1 \cdot \left(\psi \nabla_1 \frac{1}{|\underset{\sim}{R}|}\right) - \psi \nabla_1^2 \frac{1}{|\underset{\sim}{R}|}\right\} d(\text{vol.})$$

$$= \frac{\mu}{h}\psi(\underset{\sim}{r}) + \frac{\mu}{4\pi h} \int_{\text{vol.}} \nabla_1 \cdot \left(\psi \nabla_1 \frac{1}{|\underset{\sim}{R}|}\right) d(\text{vol.}) \tag{II-40}$$

If one uses the divergence theorem on the second integral and sets $\Psi = 0$ on the end edges of the cylinder, one has

$$B_\rho^I(\underset{\sim}{r}) = \frac{\mu}{h}\psi + \frac{\mu}{4\pi h} \int_{\text{outer}} \psi \frac{\partial}{\partial\rho'} \frac{1}{|\underset{\sim}{R}|} \, d(\text{area}')$$

$$- \frac{\mu}{4\pi h} \int_{\text{inner}} \psi \frac{\partial}{\partial\rho'} \frac{1}{|\underset{\sim}{R}|} \, d(\text{area}') \tag{II-41}$$

On the middle surface of the cylinder one obtains, by setting $\rho = a$ in the above expression,

$$B_\rho^I(a,\phi,z) = \frac{\mu}{h}\psi + \frac{\mu}{4\pi h}\int_{\text{outer}} \frac{\psi(a,\phi',z')[a\cos\theta - (a+\frac{h}{2})](a+\frac{h}{2})d\theta dz'}{\{[a\cos\theta - (a+\frac{h}{2})]^2 + a^2\sin^2\theta + (z-z')^2\}^{3/2}}$$

$$- \frac{\mu}{4\pi h}\int_{\text{inner}} \frac{\psi(a,\phi',z')[a\cos\theta - (a-\frac{h}{2})](a-\frac{h}{2})d\theta dz'}{\{[a\cos\theta - (a-\frac{h}{2})]^2 + a^2\sin^2\theta + (z-z')^2\}^{3/2}} \quad \text{(II-42)}$$

when $\underset{\sim}{I}$ is independent of the variable z, the self field becomes

$$B_\rho^I(a,\phi,0) = \frac{\mu}{h}\psi + \frac{\mu}{2\pi}(\frac{a}{h}+\frac{1}{2})\int_0^{2\pi} \frac{\psi(\theta)[a\cos\theta - (a+\frac{h}{2})]}{a^2 + (a+\frac{h}{2})^2 - 2a(a+\frac{h}{2})\cos\theta}d\theta$$

$$- \frac{\mu}{2\pi}(\frac{a}{h}-\frac{1}{2})\int_0^{2\pi} \frac{\psi(\theta)[a\cos\theta - (a-\frac{h}{2})]}{a^2 + (a-\frac{h}{2})^2 - 2a(a-\frac{h}{2})\cos\theta}d\theta \quad \text{(II-43)}$$

One can show that when $\Psi = c$, a constant everywhere, or $\underset{\sim}{I} = 0$, then

$$B_\rho^I = \frac{\mu c}{h}\{1 + \frac{1}{4\pi}\int_{-\infty}^{\infty}\int_0^{2\pi} \frac{[a\cos\theta - (a+\frac{h}{2})](a+\frac{h}{2})}{\{[a\cos\theta - (a+\frac{h}{2})]^2 + a^2\sin^2\theta + (z-z')^2\}^{3/2}}d\theta dz$$

$$- \frac{1}{4\pi}\int_{-\infty}^{\infty}\int_0^{2\pi} \frac{[a\cos\theta - (a-\frac{h}{2})](a-\frac{h}{2})}{\{[a\cos\theta - (a-\frac{h}{2})]^2 + a^2\sin^2\theta + (z-z')^2\}^{3/2}}d\theta dz$$

$$= \frac{\mu c}{h}\{1 - 1 + 0)$$

$$= 0$$

as it should be.

The same boundary conditions as in the flat plate case also apply to cylindrical shells. The current may be calculated from (II-32) after Ψ is determined. Pressure and temperature may be computed using (II-29) and (II-30).

Coupled Magnetomechanics

The complete set of field equations and boundary conditions for coupled magnetothermomechanics has been presented in the first section. The finite element Galerkin technique may be applied to reduce them to a set of nonlinear algebraic equations. Although all the coupling effects are preserved in the finite element equations, this approach does not seem to be practically feasible. The reasons are obvious. Firstly, the three-dimensional nature of the problem cannot be avoided. Both the conductor and the surrounding space need to be treated, and some fictitious boundary conditions assumed at some far away distance. This makes the storage and computational efforts needed to solve these nonlinear equations formidable. Secondly, the geometric and time characteristics of the problem cannot be easily represented. Consequently, it will be difficult to study the roles of some physical parameters in practical problems. The complete field approach is not emphasized in this research work; therefore, the finite element formulation of this approach will not be presented here.

The stream function method, on the other hand, averages the current through the thickness and represents it on the mid-surface of the sheet-type conductors. The problem is therefore reduced to a two-dimensional one. This method employs the current-sheet nature of the eddy-current distribution, and is parallel in spirit to the plate and shell theories of elasticity. A definition of the mid-surface is needed in this method. All the physical quantities are calculated and represented on it. This nature of the stream function approach makes it intrinsically Lagrangian. The incorporation of the large deformation analysis of structure and the transient eddy current calculation seems natural in this light, although some kind of surface interpolation may be needed to represent the deformed structure in the intermediate

stages. A possible solution procedure for large deformation analysis of the coupled magnetomechanics using stream function method is shown in Fig. II-4.

From the practical point of view, magnetomechanical problems may be classified into several groups according to the difference in time scales between mechanical and electromagnetic field problems. In the impulse loading problems, such as electromagnetic metal forming, impulse durations of $\sim 10^{1}$ μsec and strain rates of $\sim 10^{4}\text{sec}^{-1}$ have been reported [19]. Since the fundamental period of the conductor structure is much higher than the duration of the pulse, these problems are best treated as initial velocity problems. The nonlocal eddy current effect is expected to be important in this case and is definitely needed for the accurate calculation of the pressure. The mechanical part of the problem in this case is usually one of dynamic plasticity.

When the duration of the pulse, or the period of the harmonic driving current, is comparable with the fundamental period of the structure, most of the coupling will occur through the displacement of the structure. The nonlocal effect will be small in this case, because the eddy current will have enough time to diffuse. A much simpler problem may then be obtained by dropping the nonlocal effect of the eddy current. If the displacement is small so that the original configuration may be used for reference for both structural and eddy current problems, two sets of linear matrix equations may be written for structural and eddy current problems separately. The coupling of the magnetic field and the motion of the structure in this case appears on the right hand side of the equations only.

The most difficult coupling problem comes from the cases in between the above two extremes, i.e., when the frequency of the field is high and the

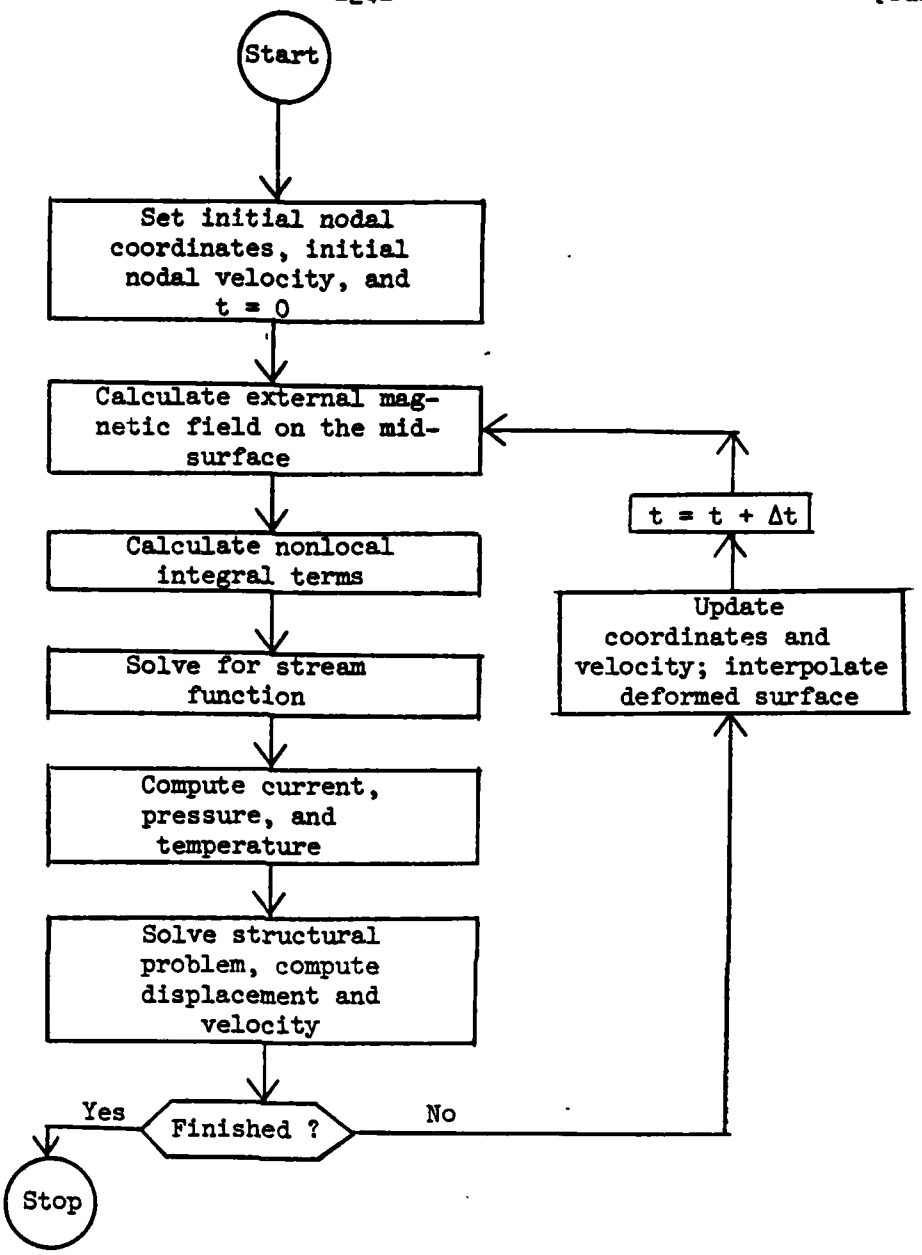

Figure II-4. A Possible Algorithm for Large-Deformation, Coupled Magnetomechanics.

duration of the pulse long enough to cause large deformations. Examples of these problems may be found in the design of fusion reactors during the starting and shut-off periods. The full power of the algorithm shown in Fig. II-4 may be needed for these problems.

Other problems of interest include the coupling between field and the rigid body motion of the conductor, such as that of magnetic transportation. A judicious choice of the type of magnetomechanical coupling is therefore essential. For plate and shell type problems, the stream function method is believed to provide a more convenient way to model the various coupling effects.

III. ONE-DIMENSIONAL CODE FOR FLAT PLATES

In this chapter the finite element Galerkin formulation for the problems of one-dimensional, steady-state harmonic currents in long plates is described. The treatment of the nonlocal integral term is briefly discussed. The capabilities of program ONED, a fortran code developed based on this formulation, is then introduced. The input and output of program ONED are finally described.

Formulation

When the current I is independent of y, eq. (II-27) has the following form:

$$\frac{\partial^2\psi}{\partial x^2} - \sigma\mu\frac{\partial\psi}{\partial t} + \frac{1}{2\pi}\sigma\mu h\int_{-A}^{A}\frac{\frac{\partial\psi}{\partial t}}{(X'-X)^2+(\frac{h}{2})^2}dX' = \sigma h\frac{\partial B_z^o}{\partial t} \qquad \text{(III-1)}$$

For steady-state harmonic currents in the plate, this equation may be non-dimensionalized into

$$\frac{d^2\phi}{dx^2} - iR\phi + i\frac{R}{2\pi}\int_{-a}^{a}\frac{\phi}{(\xi-x)^2+\frac{1}{4}}d\xi = iRB(x) \qquad \text{(III-2)}$$

in which x and ξ are distances across the width nondimensionalized with respect to the thickness h; $\psi = \phi I^o e^{i\omega t}$; $B_z^o = (\mu/\Delta)B(x)I^o e^{i\omega t}$; the magnetic Reynolds number $R = \omega\mu\sigma h^2$, which is related to the skin depth δ through $R = 2(h/\delta)^2$; I^o is the current in a nearby exciter coil; 2A is the width of the plate; and 2a the nondimensionalized width.

The finite element Galerkin method is used to solve the integro-differential eq. (III-2). ϕ is approximated globally and locally by piece-wise linear models

$$\phi = \sum_{k=1}^{G} M_k\phi_k \qquad \text{(III-3)}$$

$$\phi^e = \sum_{k=1}^{2} N_k^E\phi_k \qquad \text{(III-4)}$$

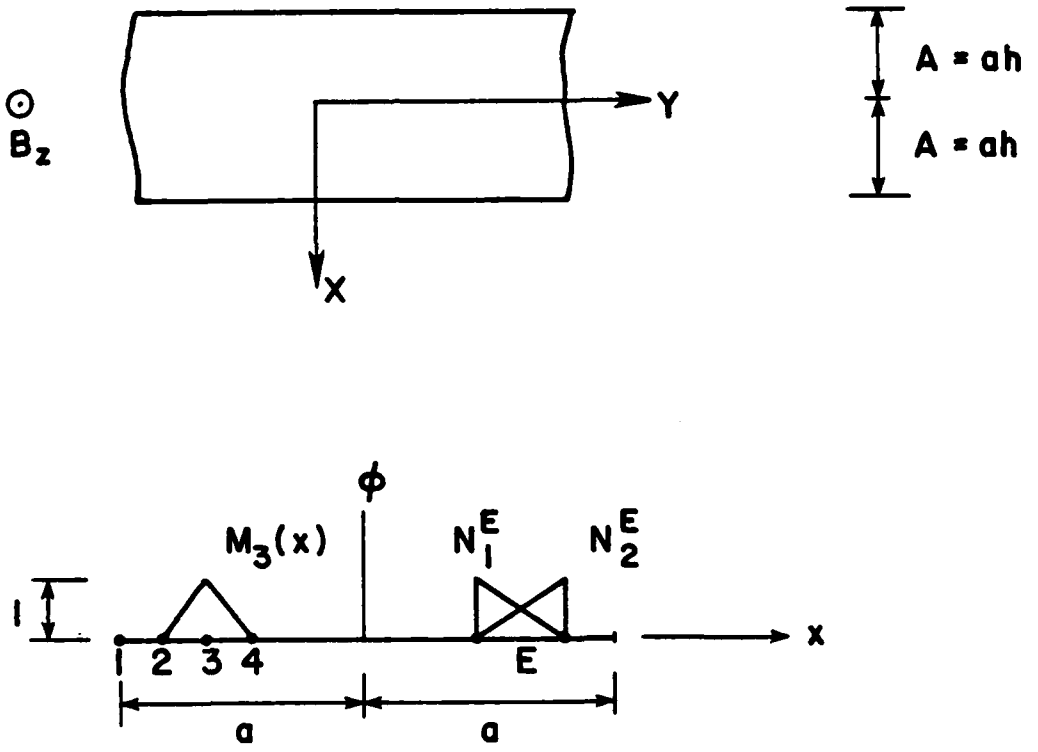

Figure III-1. Notation, Sign Conventions, and Shape Functions for One-Dimensional Flat-Plate Problems.

in which G is the total number of nodal points, the superscript E denotes the E-th element, and M_k are the global interpolation functions generated from the local linear element shape functions N_k^E. The linear algebraic equations for each element are

$$- \sum_{k=1}^{2} S_{jk}^E \phi_k - i \sum_{k=1}^{2} P_{jk}^E \phi_k + i \sum_{k=1}^{G} Q_{jk}^E \phi_k = i R_j^E \qquad \text{(III-5)}$$

in which

$$S_{jk}^E = \int_E \frac{dN_j^E}{dx} \frac{dN_k^E}{dx} dx \; ; \; P_{jk}^E = R \int_E N_j^E N_k^E dx$$

$$Q_{jk}^E = \frac{R}{2\pi} \int_{-a}^{a} M_k(\xi) W_j^E(\xi) \, d\xi \; ; \; R_j^E = R \int_E N_j^E B dx \qquad \text{(III-6)}$$

the weighting functions W_j^E used in calculating the integral term is

$$W_j^E(\xi) = \int_E \frac{N_j^E(x)}{(\xi - x)^2 + \frac{1}{4}} dx \qquad \text{(III-7)}$$

Both (III-6) and (III-7) are integrated analytically. The resulting global matrix is complex, nonsymmetric, and fully populated. The usual limited connectivity (banded matrix) finite element representation is lost due to the nonlocal nature of the problem.

When the frequency of the external magnetic field is low, the effect of the self field is small. The solution in this case will approach the local solution obtained by dropping the second and third terms on the left hand side of (III-2). When the frequencies is high, the distribution of the eddy current is primarily influenced by the self field. The solution will approach the one obtained by dropping the first term on the left of (III-2).

The solution so obtained is an asymptotic value for the high frequency limit, and is called the image solution in the literature.

Capabilities of the Program ONED

A Fortran program ONED has been developed based on eqs. (III-5) - (III-7). It is designed to perform the following calculations:

(1) local solutions of stream function, current, temperature, and pressure,

(2) nonlocal solutions of stream function, current, temperature, and pressure,

(3) image solution of stream function, current, temperature, and pressure.

To perform the calculations necessary to construct a spectrum, ØNED performs the above calculations for any number of magnetic Reynolds numbers in one run. Multiple load cases (up to 10) are allowed. Each load case will be solved for all the magnetic Reynolds numbers specified for that run.

Presently, ONED can handle uniform magnetic field cases and cases where the fields are generated by any number of conductor wires parallel to the plate. The strengths and senses of the currents and the positions of the wires may be different. Space has also been left to include other types of exciting fields in the program.

Input

Program ONED takes the geometric information of the plate and magnetic field source information as input. The total numbers of nodal points, load cases, parameter sets, and the plotting option of the output must be specified on the master input card. Nodal point information may be generated for portions of the mesh that are uniform.

The type of source of magnetic field is specified. No other information is needed for uniform magnetic field. For the parallel wire cases, the positions, senses, and the relative strengths of the currents in each wire must be input subsequently.

All the input data must be nondimensionalized according to the conventions presented in the formulation.

Output.

Values of the stream function, eddy current, temperature induced in a half-cycle of the current, and time-averaged magnetic pressure exerted on the plate are produced as output of the program. The stream function and eddy current are calculated in complex form. The stream function values are calculated at the nodal points of the mesh, while the current, temperature, and pressure are evaluated at the centroids of the elements. The stream function and eddy current are given in complex form, and the modulus and phase angle are calculated for the eddy current. Values of the modulus and phase angle for different frequencies may be used to generate the spectrum of the current at any point on the plate. These curves and the spectrum of the exciting current may be used to calculate the transient current at the point by fast Fourier transform techniques.

All the outputs of the program may be plotted out using a printer-plotter subroutine. This capability is optional and can be specified in the input.

In this program the local solutions are printed out and plotted parallel to the nonlocal solutions for comparison. When there are several load cases, the results are printed out in groups in the sequence of the load numbers. In the multiple parameter (frequency) cases, this is done for each Reynolds number. Title lines will be printed for each parameter to distinguish the different groups of output. Image solutions, which are independent of the

Reynolds number, are printed out last in the sequence of load cases.

IV. TWO-DIMENSIONAL CODE FOR FLAT PLATES

The finite element Galerkin formulation for the two-dimensional problems of steady-state, harmonic currents in flat plates is presented first. The treatment of the nonlocal integral term is then described in some detail. Program TWOD, developed based on this formulation, is then introduced. The input and output of TWOD are described at the end.

Formulation

For steady state, harmonic current in a flat plate plate, (II-27) may be nondimensionalized into the following form

$$\nabla^2\phi - i2\pi R\phi + iR \int_{\text{area}} \frac{\phi(\xi,\eta)}{[(x-\xi)^2 + (y-\eta)^2 + 1]^{3/2}} d\xi d\eta = i2\pi R\theta(x,y) \qquad \text{(IV-1)}$$

in which the coordinates are nondimensionalized with respect to half the thickness $(\frac{h}{2})$; $\psi = (\frac{hB}{2\mu})\phi e^{i\omega t}$; $B_z^o = (\frac{B}{2})\theta e^{i\omega t}$; the magnetic Reynolds number is $R = \frac{\omega\mu\sigma h^2}{8\pi}$, which is related to skin depth δ through $R = \frac{1}{4\pi}(\frac{h}{\delta})^2$; and B is the reference magnetic field.

The finite element Galerkin method is used to solve (IV-1). ϕ is approximated globally and locally by

$$\phi = \sum_{k=1}^{G} M_k \phi_k \qquad \phi^E = \sum_{k=1}^{6} N_k^E \phi_k^E \qquad \text{(IV-2)}$$

in which G is the total number of nodal points, E denotes the Eth element, M_k are the quadratic global interpolation functions generated from the local element shape functions N_k^E. Six-node triangular elements are used here. The local element shape functions are all quadratic in this case. The element algebraic equations are

$$\sum_{k=1}^{6'} K_{jk}^E \phi_k + i \sum_{k=1}^{6} P_{jk}^E \phi_k + i \sum_{k=1}^{G} Q_{jk}^E \phi_k = iR_k^E \qquad \text{(IV-3)}$$

in which

$$K^E_{jk} = \sum_{i=1}^{6} \int_{A^E} N^E_{j,i}\, N^E_{k,i}\, dA^E \qquad \text{(IV-4a)}$$

$$P^E_{jk} = 2\pi R \int_{A^E} N^E_j\, N^E_k\, dA^E \qquad \text{(IV-4b)}$$

$$Q^E_{jk} = -R \iint_{\text{area}} M_k(\xi,\eta)\, \bar{W}^E_j\, (\xi,\eta) d\xi d\eta \qquad \text{(IV-4c)}$$

$$R^E_k = -2\pi R \int_{A^E} N^E_j \theta dA^E \qquad \text{(IV-4d)}$$

The weighting function $\bar{W}^E_j$ is given by

$$\bar{W}^E_j(\xi,\eta) = \int_{A^E} \frac{N^E_j(x,y)}{[(x-\xi)^2 + (y-\eta)^2 + 1]^{3/2}}\, dxdy \qquad \text{(IV-5)}$$

Because of the numerical difficulty associated with the sharp variation of the Kernal function in (IV-5), the weighting function is calculated analytically within the element and numerically outside the element. Eq. (IV-4c) is then integrated entirely by numerical quadrature.

Since N^E_j is quadratic, six basic integrations with numerators $1, x, y, x^2, xy$, and y^2 in (IV-5) need to be performed. To simplify the integration, each element is first mapped onto a standard triangle, which is independent of the coordinates of the nodes of the element. The integrations are then performed. The expressions obtained are then used for the calculations of (IV-5) for all the elements.

The resulting global matrix is again complex, nonsymmetric, and fully populated. Local, nonlocal, and image solutions can be calculated just as in the one-dimensional case. Eddy currents can be calculated through numerical

differentiation, and magnetic pressure and temperature evaluated after the stream function is solved.

Capabilities of the Program TWOD

A fortran program TWOD has been developed based on the formulation of eqs. (IV-3) - (IV-5). It calculates the local and nonlocal solutions of stream function, eddy current, temperature, and pressure. As of this writing, the image solution and two-dimensional graphic output capabilities remain to be implemented. Uniform magnetic field and fields due to any number of magnetic dipoles can be handled. Magnetic fields generated from some types of coils of interest will be added. Capability of analyzing for multiple frequencies is also to be implemented.

Input

The geometry of the plate and the description of the external magnetic field are the two basic forms of data needed by program TWØD. The total numbers of nodal points, load cases, and elements need to be specified. Coordinate and boundary condition must be given for each input node. Intermediate nodes may be generated for any groups of nodal points that are uniformly spaced. Element information may also be generated. Although only six-node triangles are included in the present version of TWØD, the program has been structured so that other types of elements may be added. Element group information and the master card for each element group therefore need to be input too.

The program allows for different orders of numerical integrations. Six- and seven-point formula are now provided. The order may be specified on the master element group card.

Presently two types of magnetic fields may be analyzed: the uniform field and the magnetic field due to any number of dipoles. For uniform

field no other information is needed. For dipole field the positions and the relative strengths and senses of each magnetic dipole must be given subsequently.

Output

Values of the stream function, eddy current, temperature induced in a half cycle of the current, and time-averaged magnetic pressure are produced as output. The stream function is calculated at the nodes of the finite element mesh. Current, temperature, and pressure are evaluated at the centroid of each element. The stream function and current are calculated in complex form. The modulus and phase angle of the current are evaluated in the interest of spectral analysis for the calculation of transient currents.

V. NUMERICAL RESULTS AND EXPERIMENTAL VERIFICATION

The computer programs described in the preceding two chapters have been applied to a number of problems to test and verify their validity and to demonstrate their utility for problems of scientific and practical interest. A portion of the verification process is the comparison of the computed results with experimental measurements. This chapter consists of a summary report of these numerical results.

One-Dimensional Analysis

The first test of the numerical techniques discussed in the previous sections was the calculation of induced currents in a long rectangular plate by a two-dimensional magnetic field (Figure V-1). Near the center of the plate the currents are one dimensional or are parallel to the long edges of the plate. The external magnetic field used in the test cases was that due to parallel current filaments above the plate and a uniform time dependent magnetic field. In addition to the induced current distribution across the plate, the induced temperatures and magnetic pressure distributions were calculated.

The following objectives were met with the one-dimensional program:

a) Comparison of low magnetic Reynolds number (R) results with direct quadrature of local theory.

b) Comparison of high R results with the image method.

c) Demonstration of the importance of nonlocal theory for moderate frequencies or R.

d) Comparison of finite element calculations with experimental infrared measurements.

e) Combination of the finite element (FE) results for different field frequencies with the fast Fourier transform (FFT) to predict dynamic currents and pressures.

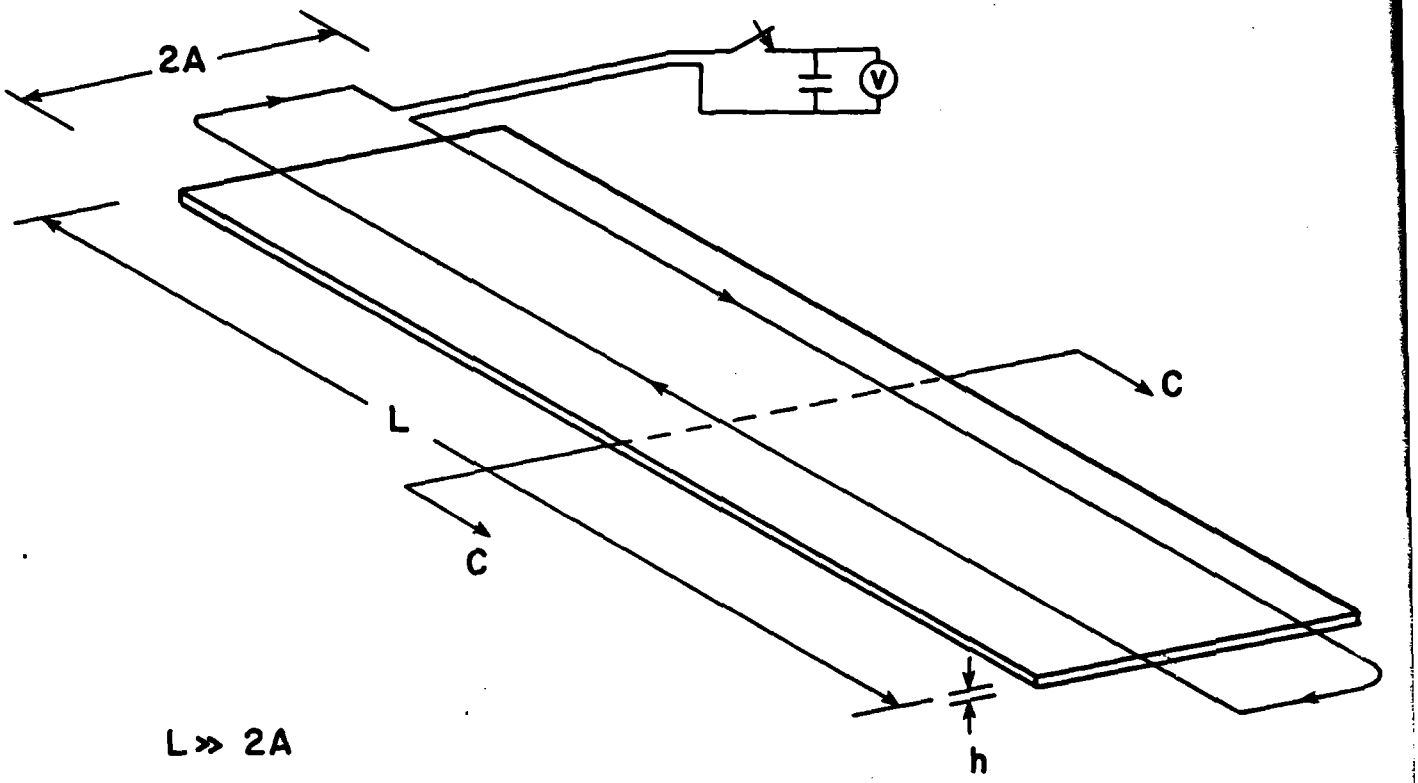

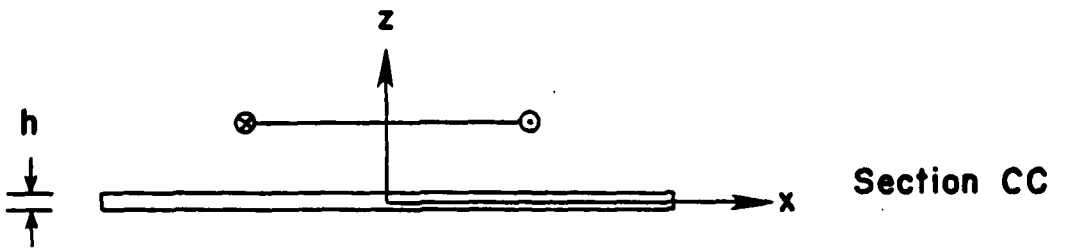

Figure V-1. Induced Currents in a Long Rectangular Plate.

f) Demonstration of the importance of the edge effect in increasing the current density and magnetic pressure.

g) Calculation of the magnetic forces on a long plate due to a tilted coil.

h) Examined the effect of a banded matrix as an approximation to the full matrix or complete nonlocal solution.

Each of these will be described in the following subsections.

Comparison of FEM with Direct Quadrature for R<<1. When R<<1 one may drop the nonlocal terms in eq. (III-2) and obtain the local theory for the stream function, i.e.

$$\nabla^2\phi = iRB(x) \qquad \text{(V-1)}$$

The solution for the one-dimensional case can be found by direct integration of a given B(x). Comparison of the low Reynolds number solution for the finite element method (FEM) and direct quadrature is shown in Figure V-2 for a pair of current filaments centered above a long conducting plate. The results show excellent agreement.

Comparison with the Image Method. When the frequency is high, i.e., R<<1, the nonlocal effects act to prevent the magnetic field from penetrating the plate. In this limit the solution can be approximated by considering an image coil below the plate with serves to cancel out the normal component of the total magnetic field (Figure V-3). The results of the one-dimensional FEM with the image coil calculation are shown in Figure V-4 and again show excellent agreement.

Nonlocal vs. Local Theory for Eddy Currents. A comparison of the local and nonlocal theories for eddy current distribution is shown in Figure V-5 for different R or frequencies. It is clear that even though

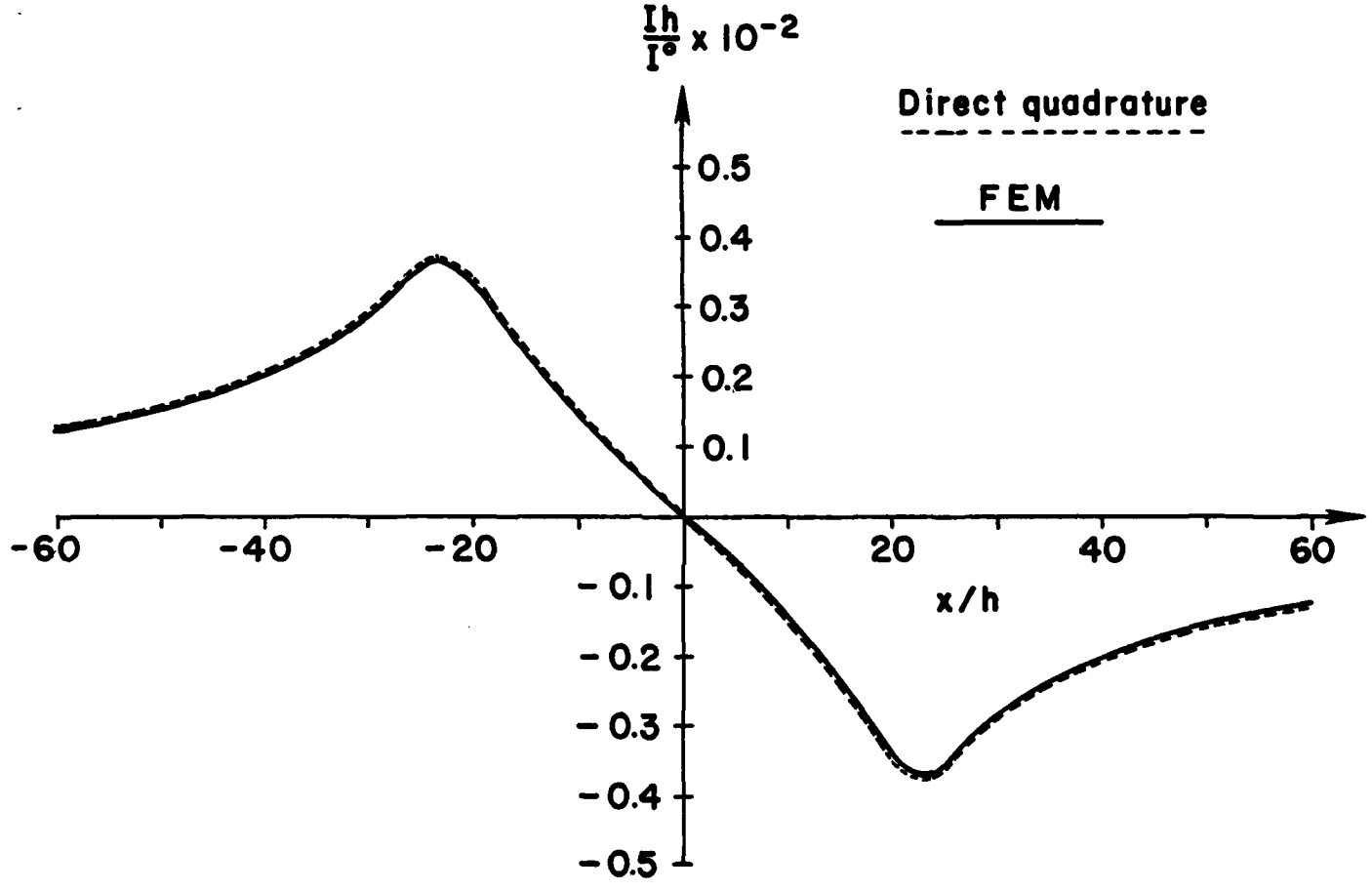

Figure V-2. Comparison of FEM and Direct Quadrature Solutions for Low R for a Pair of Current Filaments Centered Above a Long Conducting Plate (R = 0.01).

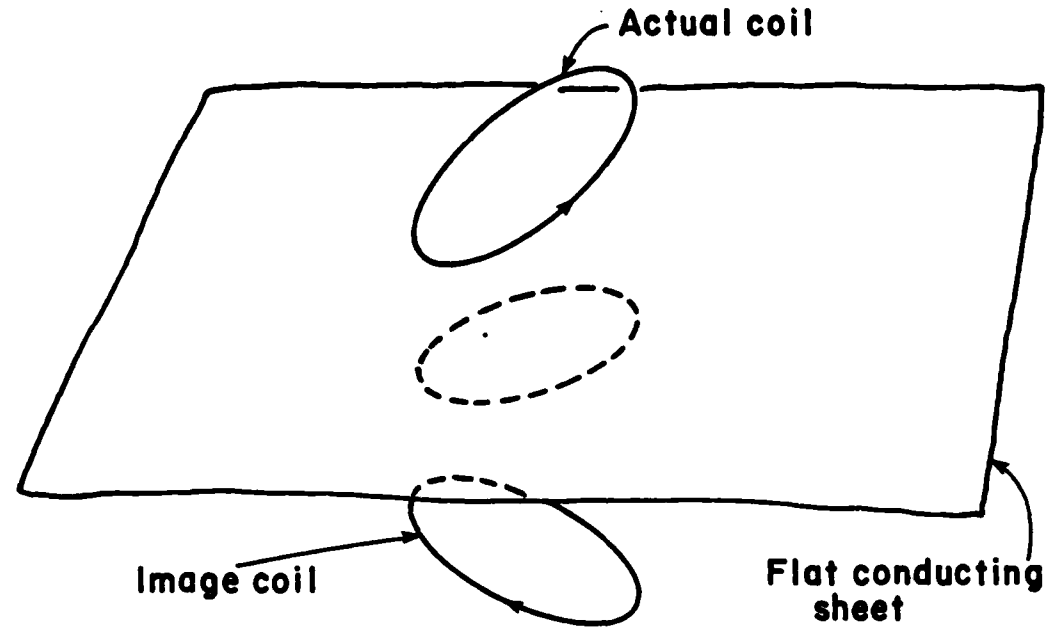

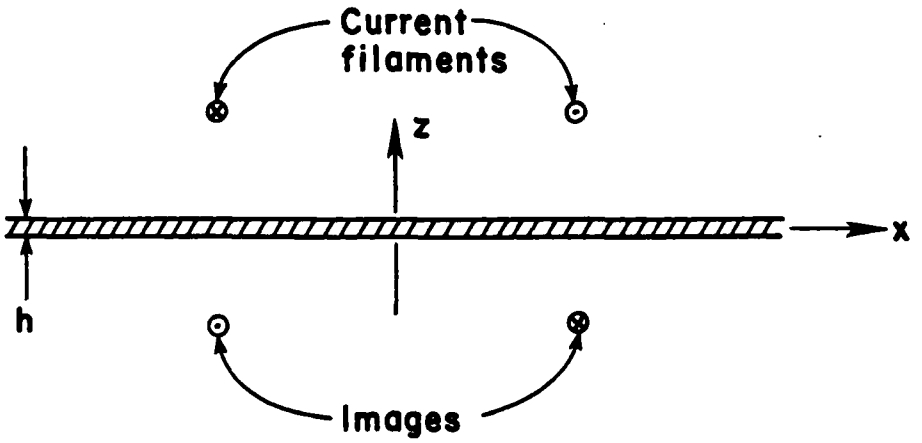

Figure V-3. The Image Method for High R.

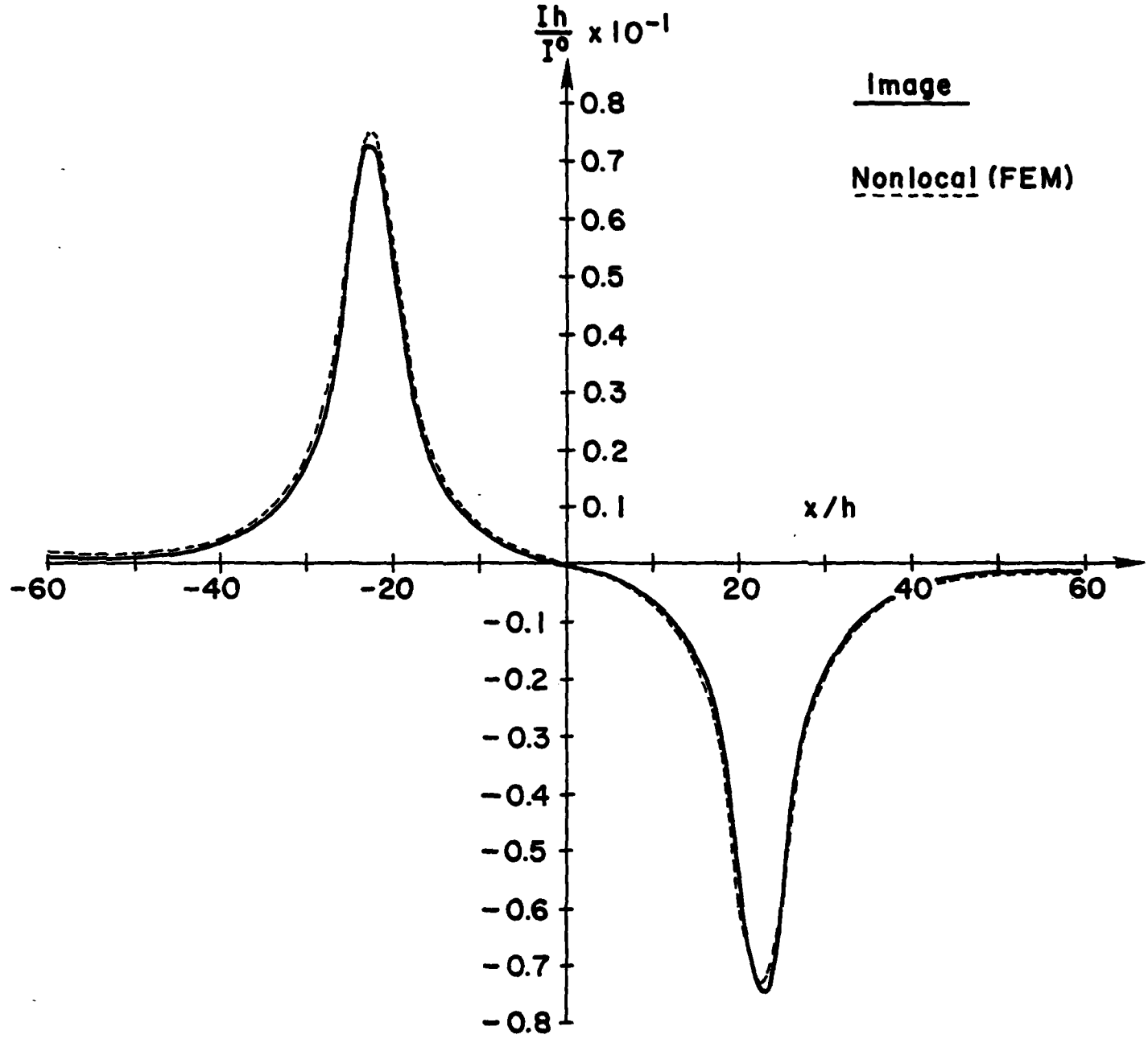

Figure V-4. Comparison of FEM and Image Method Solutions for High R for a Pair of Current Filaments Centered Above a Long Conducting Plate (R = 5).

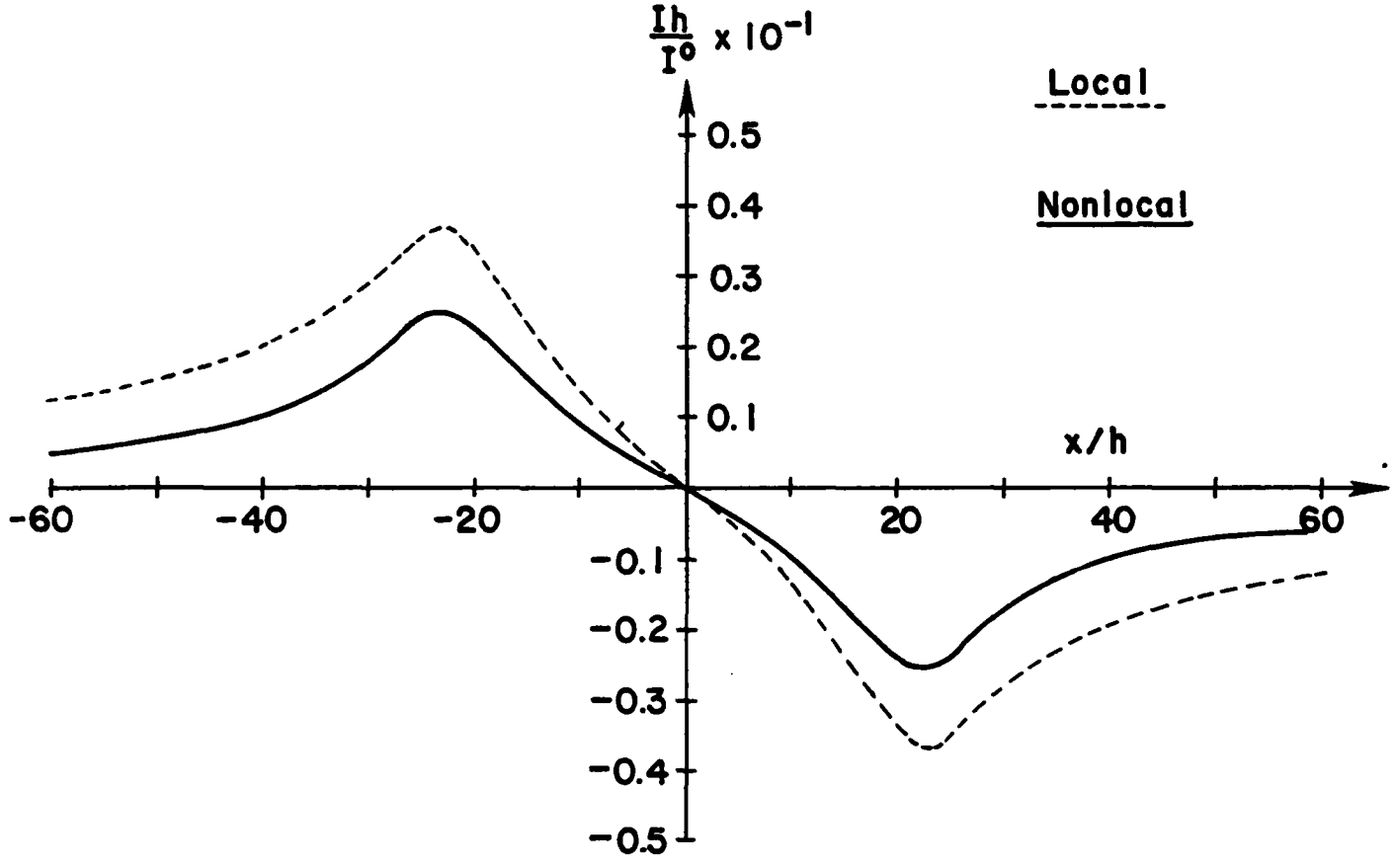

Figure V-5. Comparison of Nonlocal and Local Solutions for a Pair of Current Filaments Centered Above a Long Conducting Plate (R = 0.1).

the skin depth may be several times the thickness (R = 0.1, δ = 4.5h), the nonlocal distribution differs significantly from the local theory. The importance of the nonlocal effects is not often recognized as evidenced by the number of eddy current calculations which neglect the nonlocal contribution [16] [20].

A more fundamental difference between the nonlocal and local effects concern the magnetic pressure. When the nonlocal or self field of the induced currents is neglected, the average force on the plate for a sinusoidal current is zero. The nonlocal or self-field effects are necessary to obtain a time-averaged force on the plate between the sources of the external field (such as coils or current filaments) and the currents in the plate.

Comparison of FE Calculations with Experimental Measurements. An important feature of this research program has been the experimental verification of the numerical calculations. To check the calculations, measurements of one of several physical quantities along the surface of the plate must be made such as electric or magnetic fields, induced temperature, or magnetic pressure. Measurement of electric or magnetic fields associated with the induced currents in the plate involve taking data of a sufficient number of points to map out the current distribution. However, in recent years an infrared scanning technique has been developed which can sense the incremental temperature distribution. This technique is based on the fact that for small times after the induced currents are generated, the heat conduction can be neglected and the induced temperature is proportional to the square of the current density. The heat equation is given by

$$-\kappa\nabla^2 T + c\,\frac{\partial T}{\partial t} = \frac{J^2}{\sigma} \qquad \text{(V-2)}$$

in which κ is the thermal conductivity, and c is the heat capacity of the plate. Under appropriate conditions on the gradient of temperature and time, one may neglect the first term and write

$$T \doteq \frac{1}{c\sigma} \int_0^t J^2 dt \qquad \text{(V-3)}$$

To simulate a one-dimensional problem, a rectangular multiturn induction coil was placed parallel to a flat aluminum plate and induced temperatures were measured across the plate under the middle of the coil (Figure V-6). The two-dimensional infrared scanner used is described in Appendix A. An infrared thermogram of the temperature or J^2 pattern in the plate due to a pulsed rectangular coil is shown in Figure V-7. The induction coil has damped sinusoidal currents. Comparison of the qualitative behavior of the measured temperature and the calculated temperature distribution along the plate using an effective frequency is shown in Figures V-8 and V-9 for both high and low frequencies. Both calculated and measured data have been normalized. Excellent qualitative agreement can be seen for the coil centered above the plate (Figure V-8) and for the coil near the edge of the plate (Figure V-9).

Quantitative agreement is difficult because the calculations are for a harmonic excitation field and the experiment used pulsed current in the coil. This problem was solved by calculating the induced current density, as a function of frequency, and using a fast Fourier transform (FFT) to calculate the induced current as a function of time, as shown in Figure V-10. This data was then integrated using equation (V-3) above to calculate the temperature as a function of time at the point of maximum temperature in the plate. Using the maximum temperature in time along with the calculated distribution as in Figure V-10 a quantitative comparison of calculated and

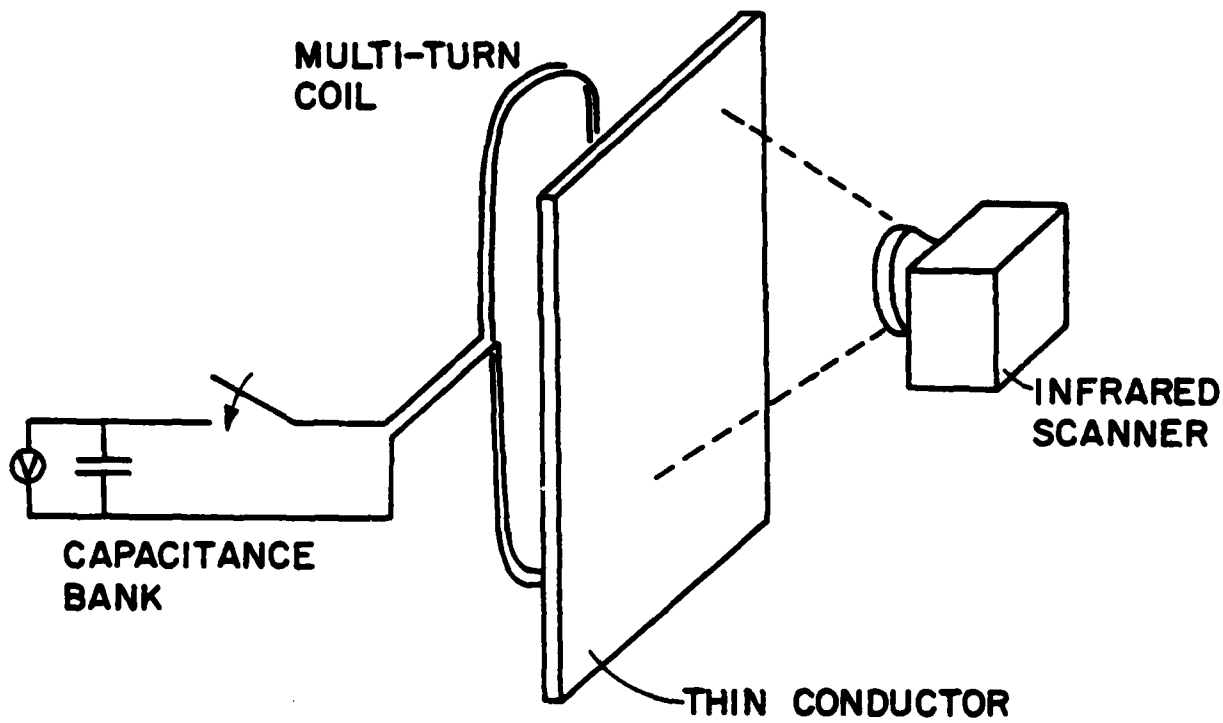

Figure V-6. Method of Detecting Eddy Current Flow Patterns in Thin Structures.

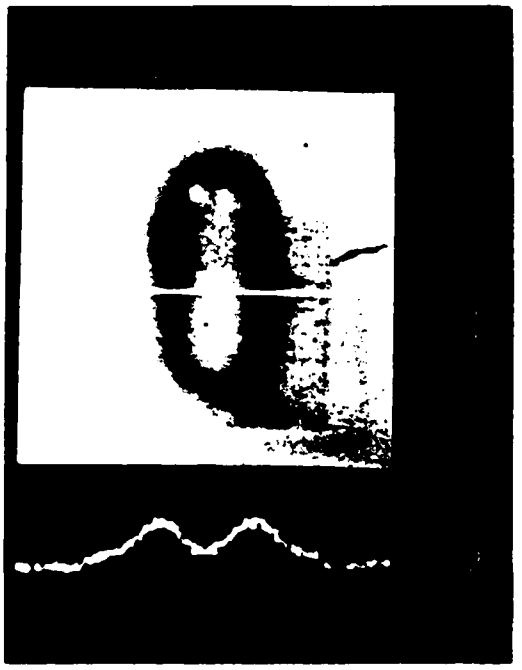

Figure V-7. Photograph of an Infrared Thermogram for Currents in a Plate as Induced by a Pulsed Rectangular Coil.

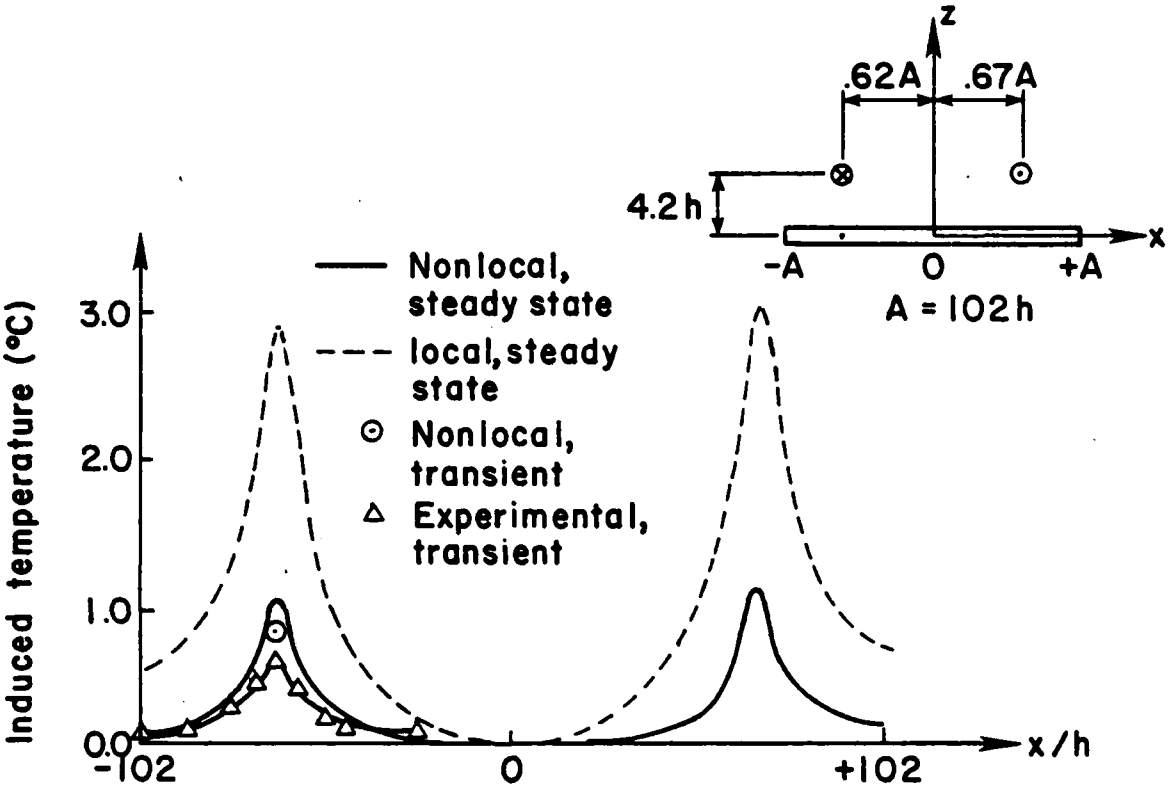

Figure V-8. Comparison of FE Solution and Measured Temperatures for a Pair of Current Filaments Centered Above a Long Conducting Plate (R = 0.071).

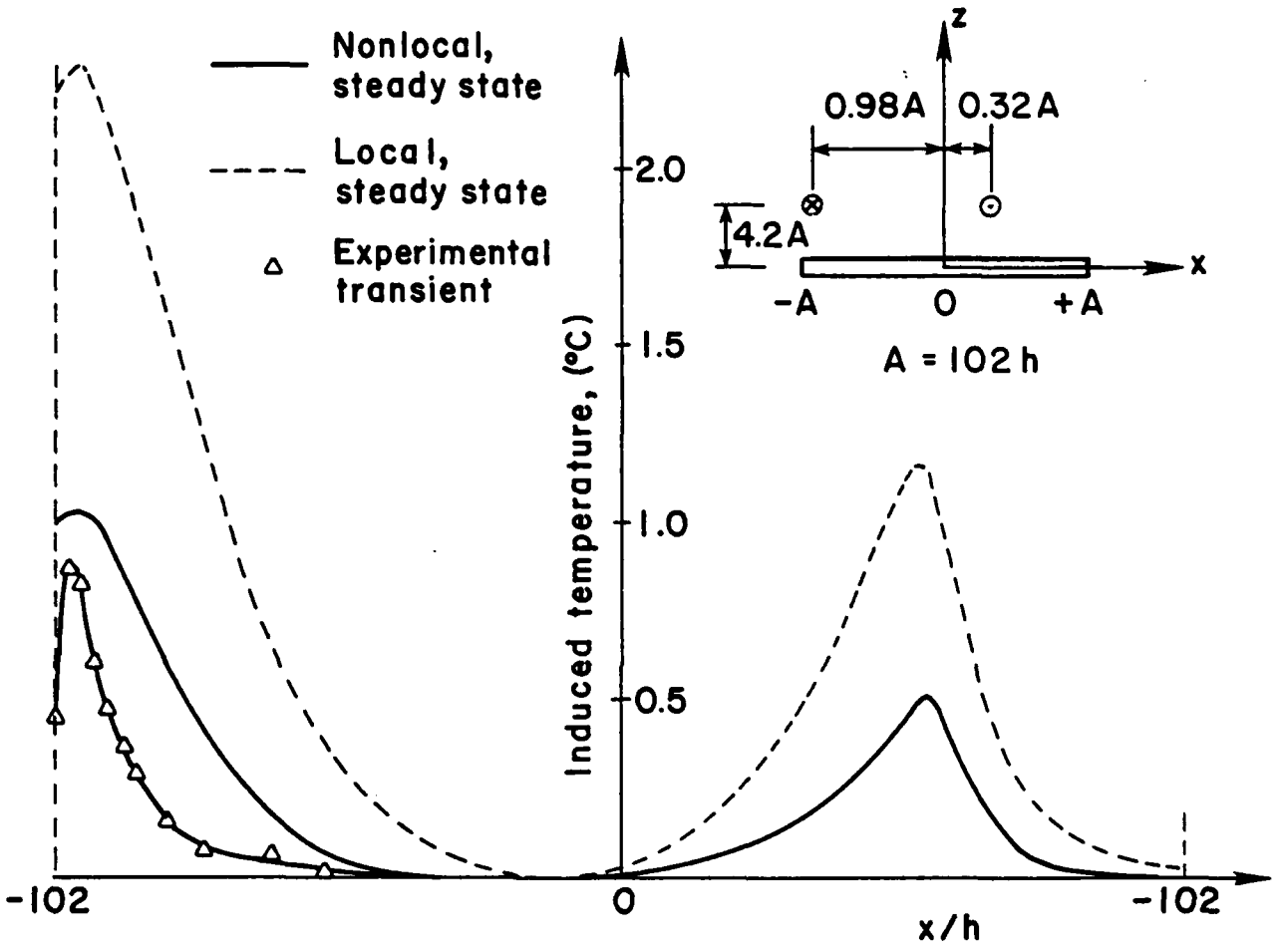

Figure V-9. Comparison of FE Solution and Measured Temperatures for a Pair of Current Filaments Nearer One Edge of a Long Conducting Plate (R = 0.074).

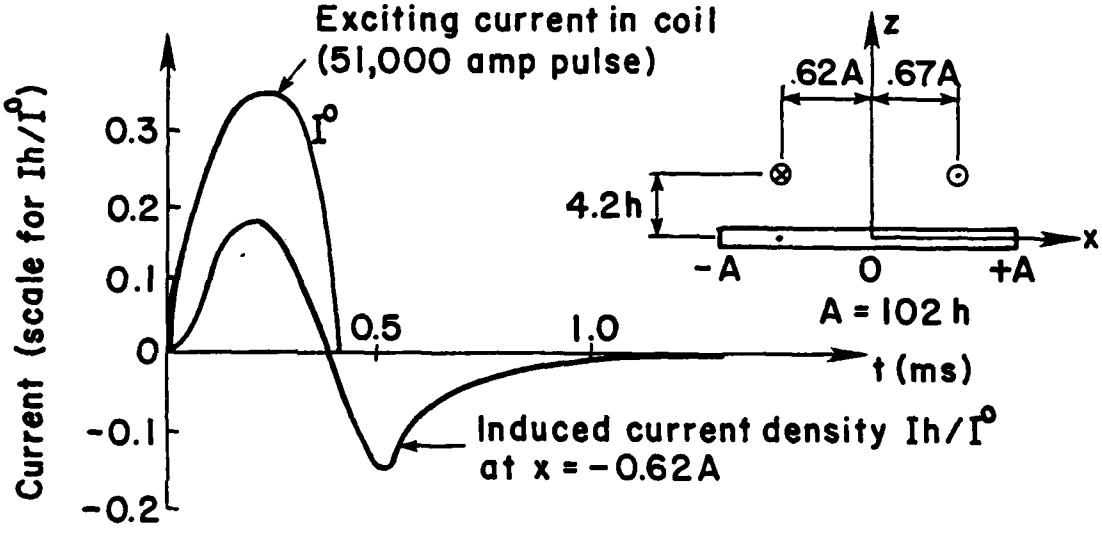

Figure V-10. Transient Exciting and Induced Currents as Functions of Time.

measured temperatures were made as shown in Figure V-8. As might be expected the measured values are about 20% below the calculated values. This may be accounted for by heat transfer effects, and the fact that the observed temperature on the back side of the plate may be different than the mean temperature across the plate.

It is believed that the difference can be accounted for by experimental error; therefore, the results are encouraging. Further experimental work may be done using a search coil technique to measure the induced current across the plate.

FE and FFT Methods for Pulsed Magnetic Fields. As discussed in the previous section, the distribution of current in the plate, as well as induced pressure and temperatures are for harmonic excitation. For pulsed or transient excitation fields $\underset{\sim}{B}^{o}(t)$, one may decompose the field into its spectral components

$$B_o f(\omega) = \frac{1}{2\pi} \int_{-\infty}^{\infty} B(t)\, e^{i\omega t} dt \qquad (V\text{-}4)$$

If the induced current is calculated as a function of frequency $J(\omega)$, for an excitation $B_o e^{-i\omega t}$, the time variation of current can be found from the integral

$$J(t) = \int_{-\infty}^{\infty} J(\omega)\, f(\omega) e^{-i\omega t} d\omega \qquad (V\text{-}5)$$

The function $J(\omega)$ was found by calculating the induced current for various frequencies using the nonlocal theory as shown in Figure V-11. A polynomial was then fitted to these points over the significant frequency domain of $f(\omega)$. The Fourier integral was then approximated by a finite sum and the summation carried out using a fast Fourier transform algorithm. The resulting time history of current in the plate is shown in Figure V-10.

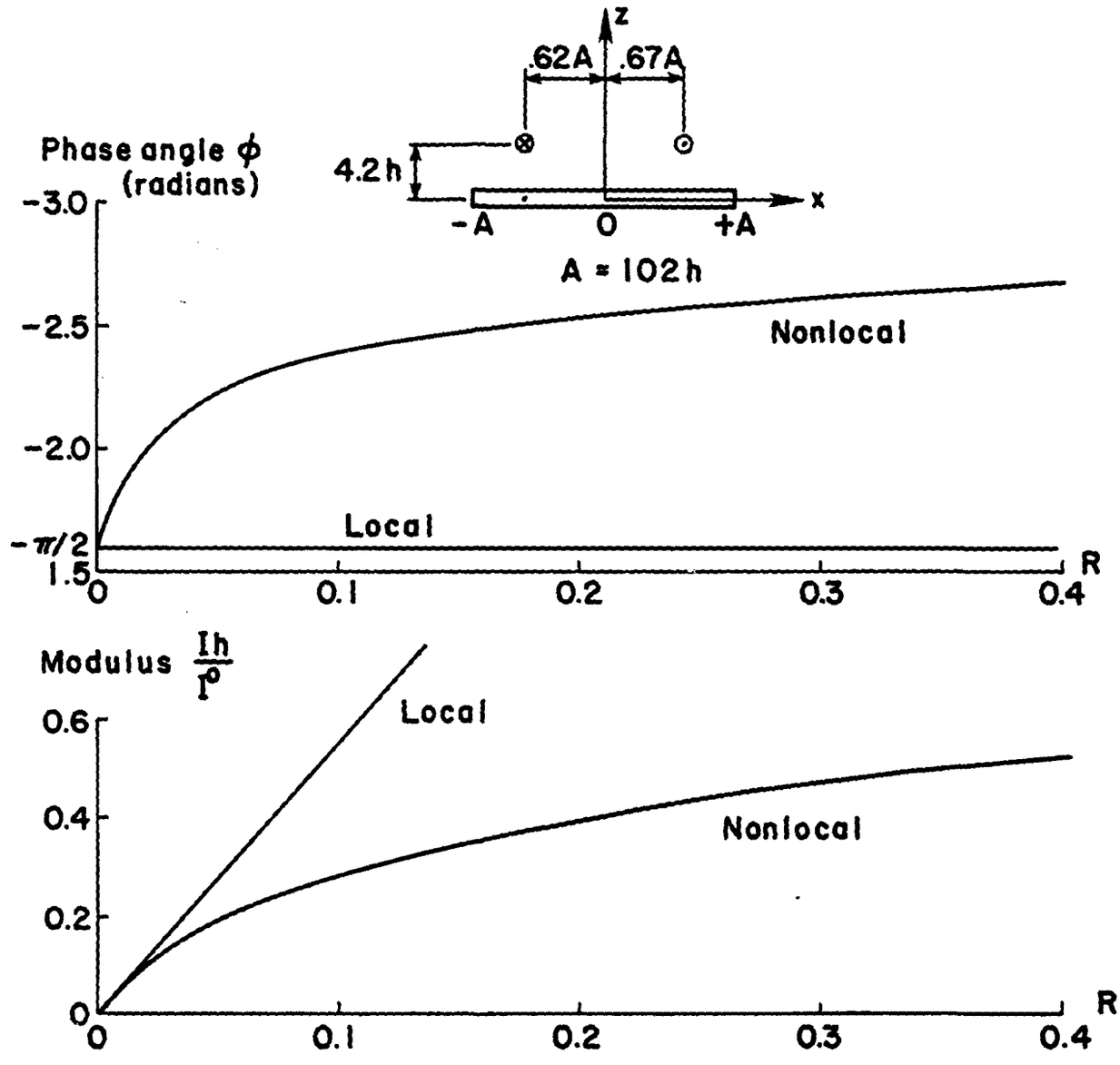

Figure V-11. Spectrum for Current at x = -0.62A for Local and Nonlocal Solutions.

From this history the magnetic force and induced temperature histories in the plate can be calculated.

Effect of Edges on Induced Eddy Currents. One of the immediate results of infrared scan experiments on induced eddy currents in plates was the observation that high current densities will occur when the excitation field is concentrated near the edges of the plates. This can be seen in Figure V-12a & b where a coil is moved closer to the edge of a rectangular plate. The results of the one-dimensional program also show a distinct edge effect for both the paired current filament induction, Figure V-9, and the uniform field induction, Figure V-13.

Pressure Distributions Due to Tilted Induction Coils. Both magnetic forming devices and magnetic levitation devices use current carrying coils near plate-like conductors. The effect of tilting the induction coil has been calculated as shown in Figures V-14 and V-15. The increased magnetic pressure under the filament close to the plate produces a moment on the plate and a restoring moment on the coil. The effect of lateral movement of the coil can also be seen in Figure V-15, and the effect of lateral movement on the restoring moment can be calculated.

Effect of Reduced Matrix Band on Nonlocal Solutions. One manifestation of the FE implementation of the nonlocal theory is that the algebraic FE equations become full rather than banded. Nevertheless, the nonlocal effects which cause this loss of banding are proportional to $1/r^2$ in which r is the distance from a self-field source point on the sheet conductor to the field point in question, eq. (III-2). One method of restricting the nonlocal effect at any field point on the sheet would be to exclude source points at distances from the field point greater than some cut-off value of r. For a uniformly spaced finite element mesh, this would yield a banded matrix,

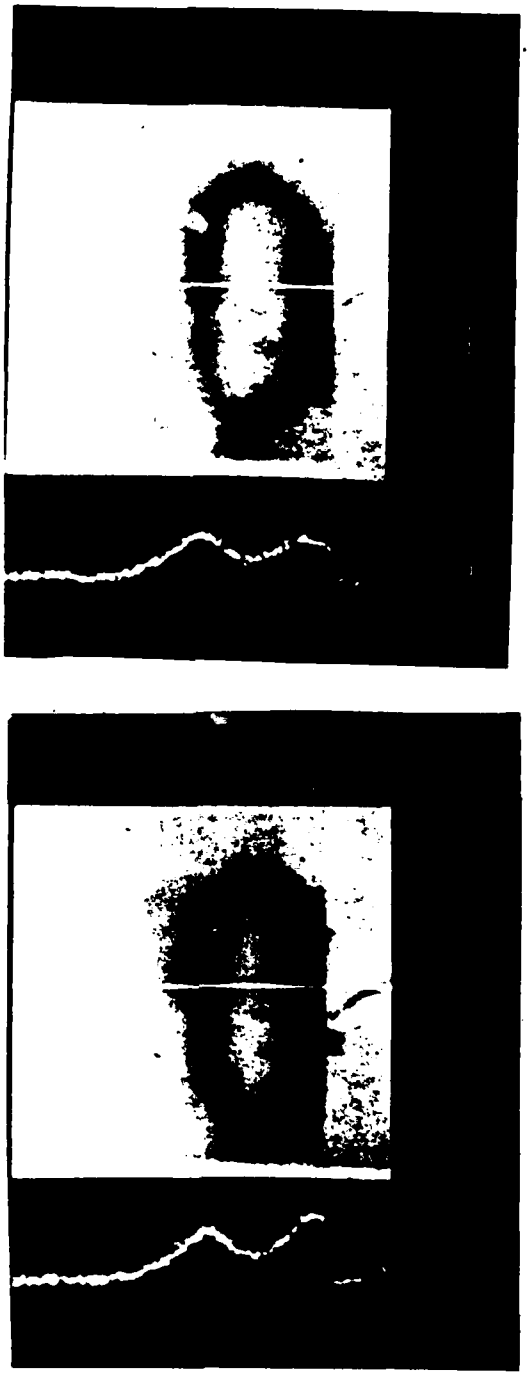

(a)

(b)

Figure V-12. Photographs Showing Effects of Edges on Induced Eddy Currents.

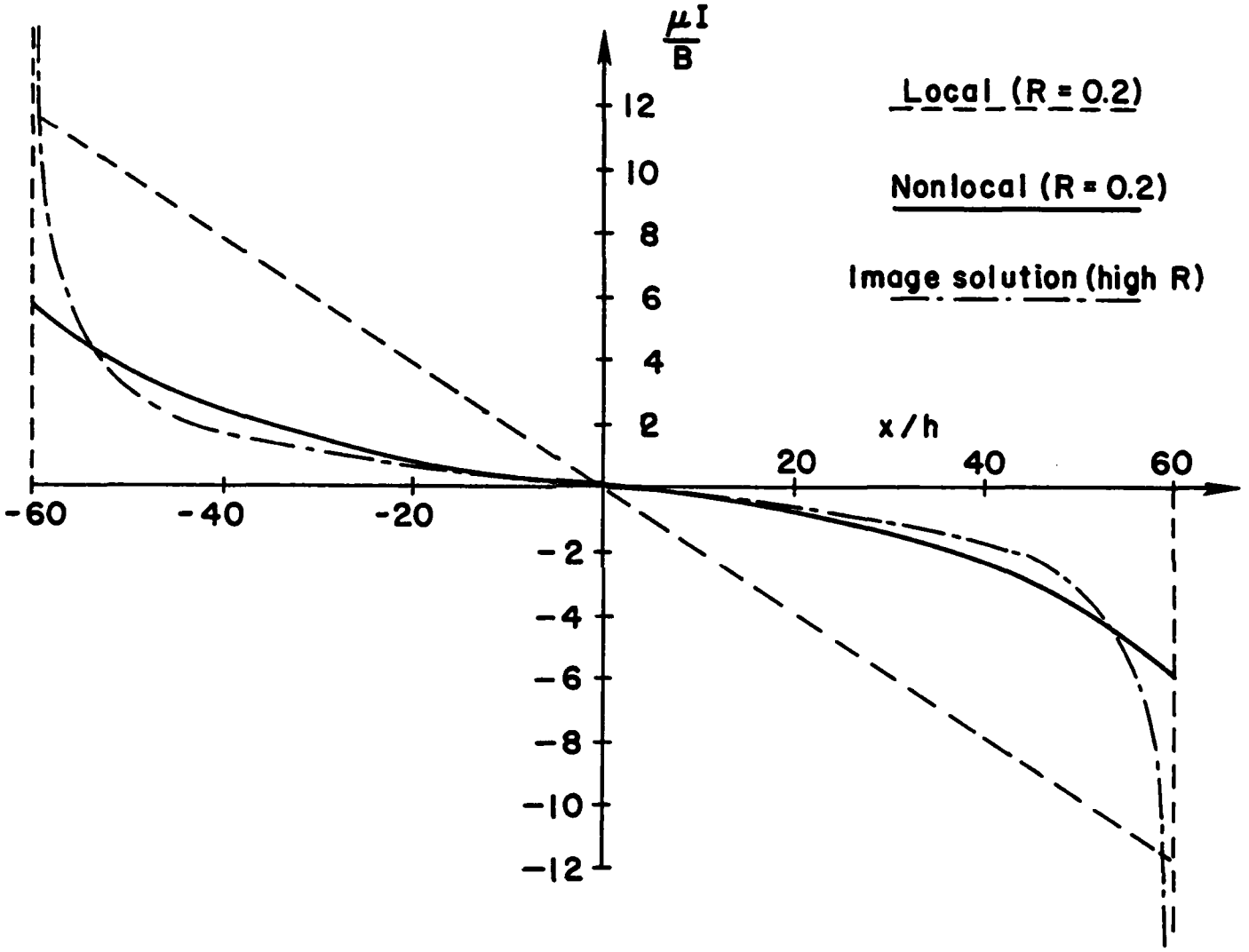

Figure V-13. Calculated Edge Effects for Uniform Induction Field.

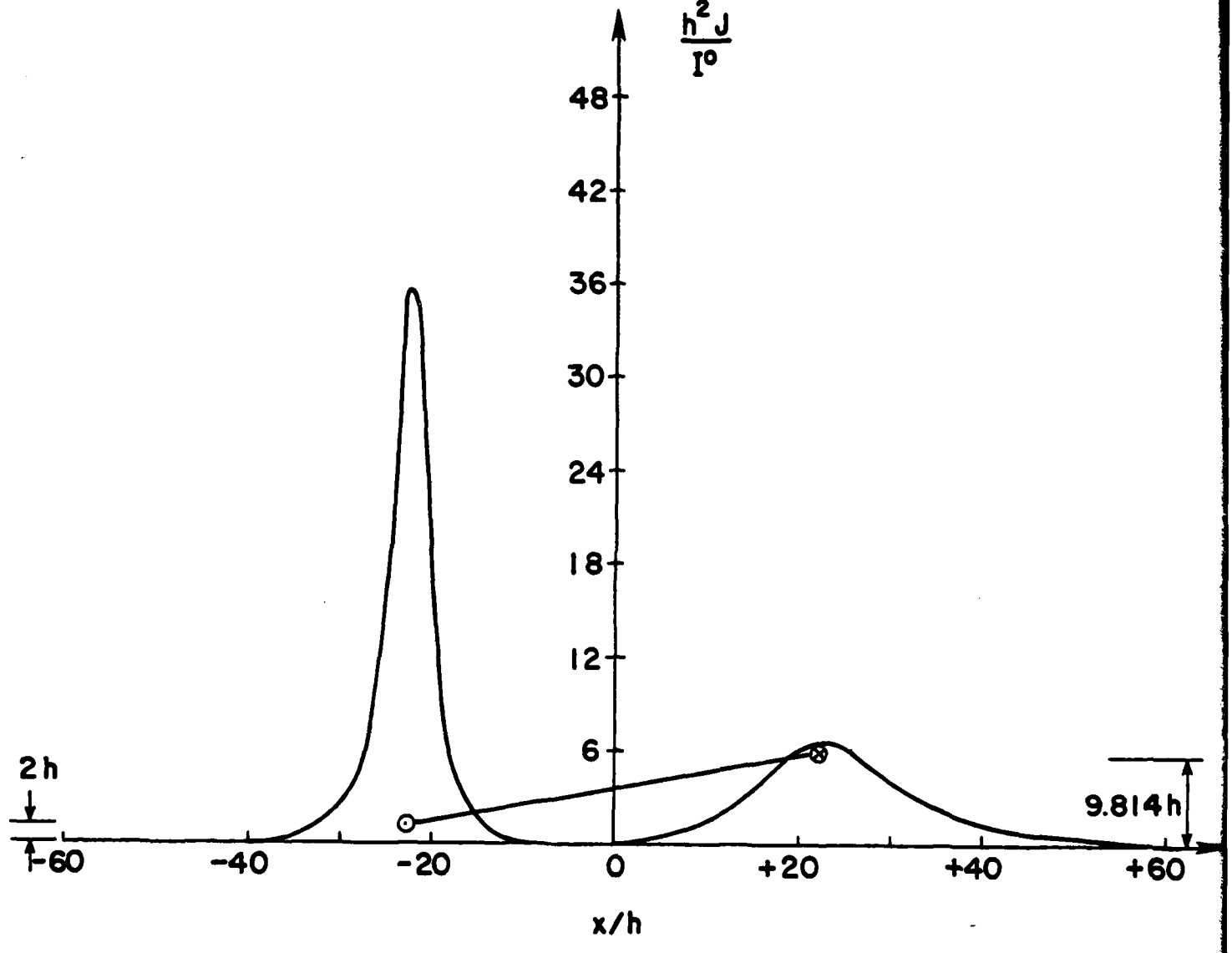

Figure V-14. Magnetic Pressures Due to a Tilted Pair of Current Filaments Centered Above a Long Conducting Plate (R = 0.07, tilt = 10°).

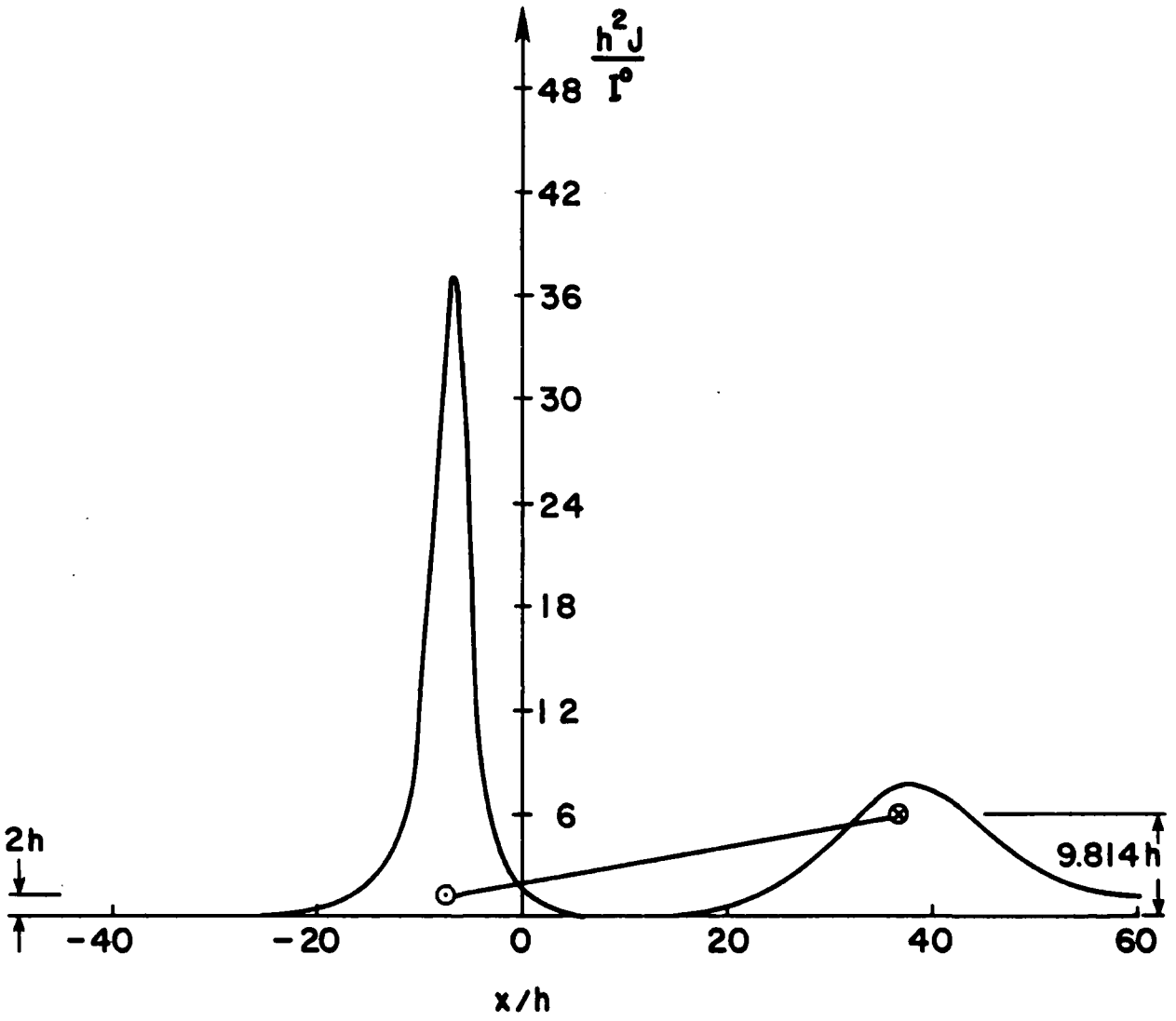

Figure V-15. Magnetic Pressures Due to a Tilted Pair of Current Filaments Nearer One Edge of a Long Conducting Plate (R = 0.07, tilt = 10°).

but the size of the band would now be determined by the cut-off distance. The choice of an appropriate cutoff distance will be dependent upon the particular problem. The solution to the restricted nonlocal problem with an appropriate cutoff distance would be negligibly different from the full nonlocal solution, and considerable savings in computation would be achieved due to a reduction in the nonlocal integrations required, eq. (III-2).

As a preliminary test of this strategy, the expedient of merely reducing the bandwidth of the FE equations was utilized by neglecting all terms outside of selected bandwidths. For the nonuniform mesh necessary for the eddy currents induced by a pair of external current filaments, this procedure is not equivalent to the selection of a cutoff distance. (A finer mesh is required under each filament). Nevertheless, as illustrated in Figure V-16, the reduction in bandwidth provides a variation in the solution that approaches the full nonlocal solution. These results provide evidence that reduced nonlocal solutions will be efficient and useful in some situations. Future research will follow up on this indication by developing criteria for the selection of appropriate cutoff distances and by implementing this strategy in computer programs.

Two-Dimensional Analysis

As described in Chapter IV, a two-dimensional finite element code has been written to predict the induced eddy currents in flat plates where the skin depth is equal to or greater than the plate thickness. This code has been partially verified in some limiting cases such as the low magnetic Reynolds number limit. In this limit the solution for the stream function reduces to a Poisson equation. For the uniform normal external magnetic field, the problem is analogous to the torsion of a shaft. In this limit, the FEM solution for a square and rectangular plate has been checked with analytical solutions

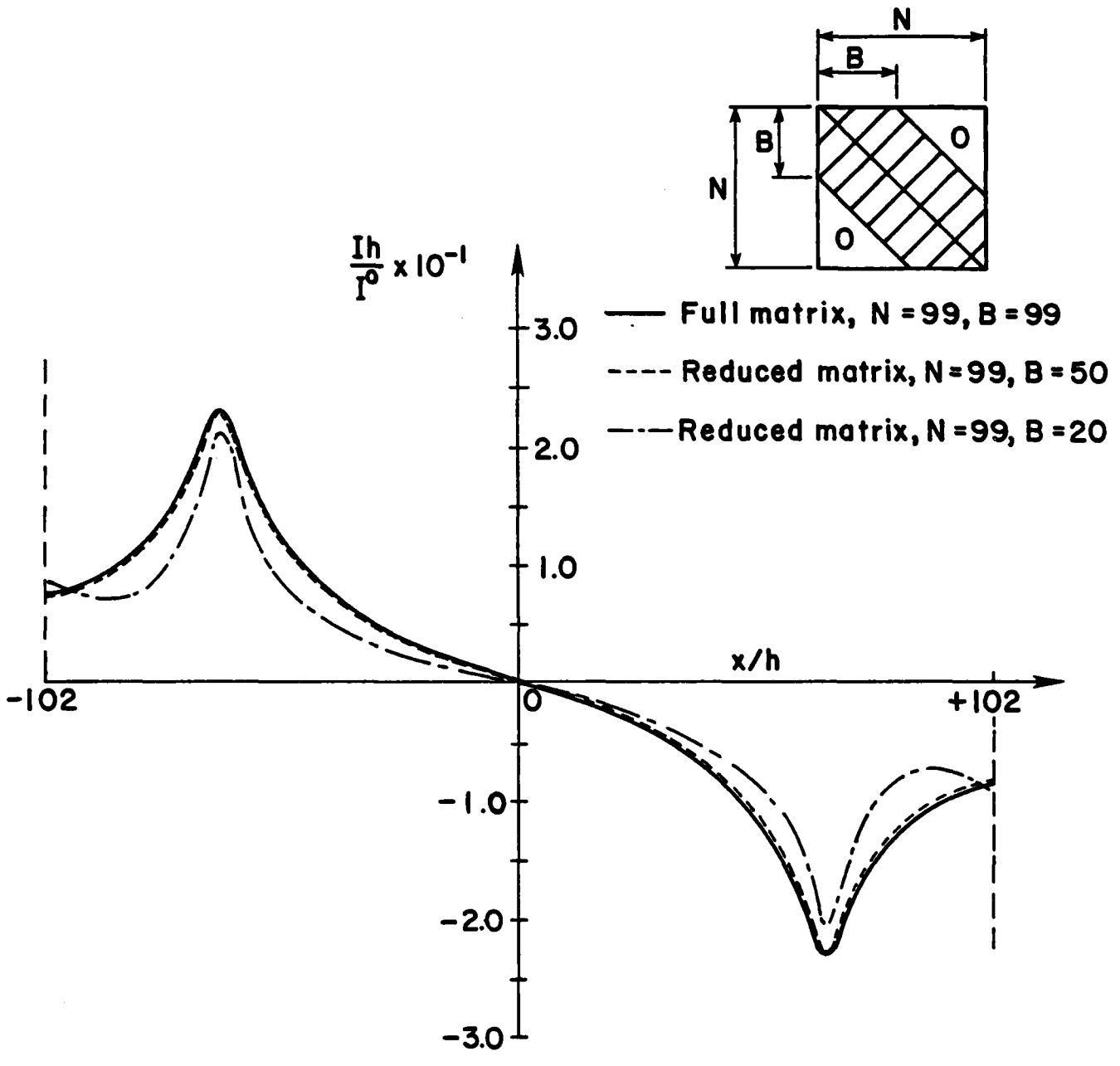

Figure V-16. Effect of Reduced Matrix Band on Nonlocal Solutions for a Pair of Current Filaments Centered Above a Long Conducting Plate (R = 0.071).

for torsion of rectangular shafts.

The stream function contours for a rectangular plate in a uniform magnetic field with sinusoidal time variation is shown in Figure V-17. The resulting comparison of induced currents across the middle of the plate has checked the one-dimensional solution in the low R limit (Figure V-18).

Nondestructive Testing (NDT) Application. One of the immediate applications of the two-dimensional results is the possibility of using induced eddy currents and infrared scanning to detect cracks and flaws in sheet-like conductors such as plates and shells. When the current flow is interrupted by a crack, the increased current concentration near the crack tips increases the induced temperature there which can be detected by an infrared scanner. Such an example is shown in Figure V-19 where the tip of the crack or slit shows up as a bright "hot spot".

The flow of current around a crack or slit in a plate was calculated using the two-dimensional code for in the large skin depth limit ($R \to 0$) for a few notch widths. The stream function contours for one case are shown in Figure V-20. These contours show the flow of current around the crack tip. Contours of constant temperature are also shown in Figure V-21. These results are in qualitative agreement with the infrared measurements since they clearly show the temperature or J^2 hot spots near the edges of the crack or slit.

This program can thus be used to develop a catalog of thermograms for various flaws, cracks, and cutouts in sheet-like conductors. Also the code can be used to calibrate eddy current probe NDT devices by predicting the change of impedance in the probe as the eddy current probe is brought near a crack or flaw.

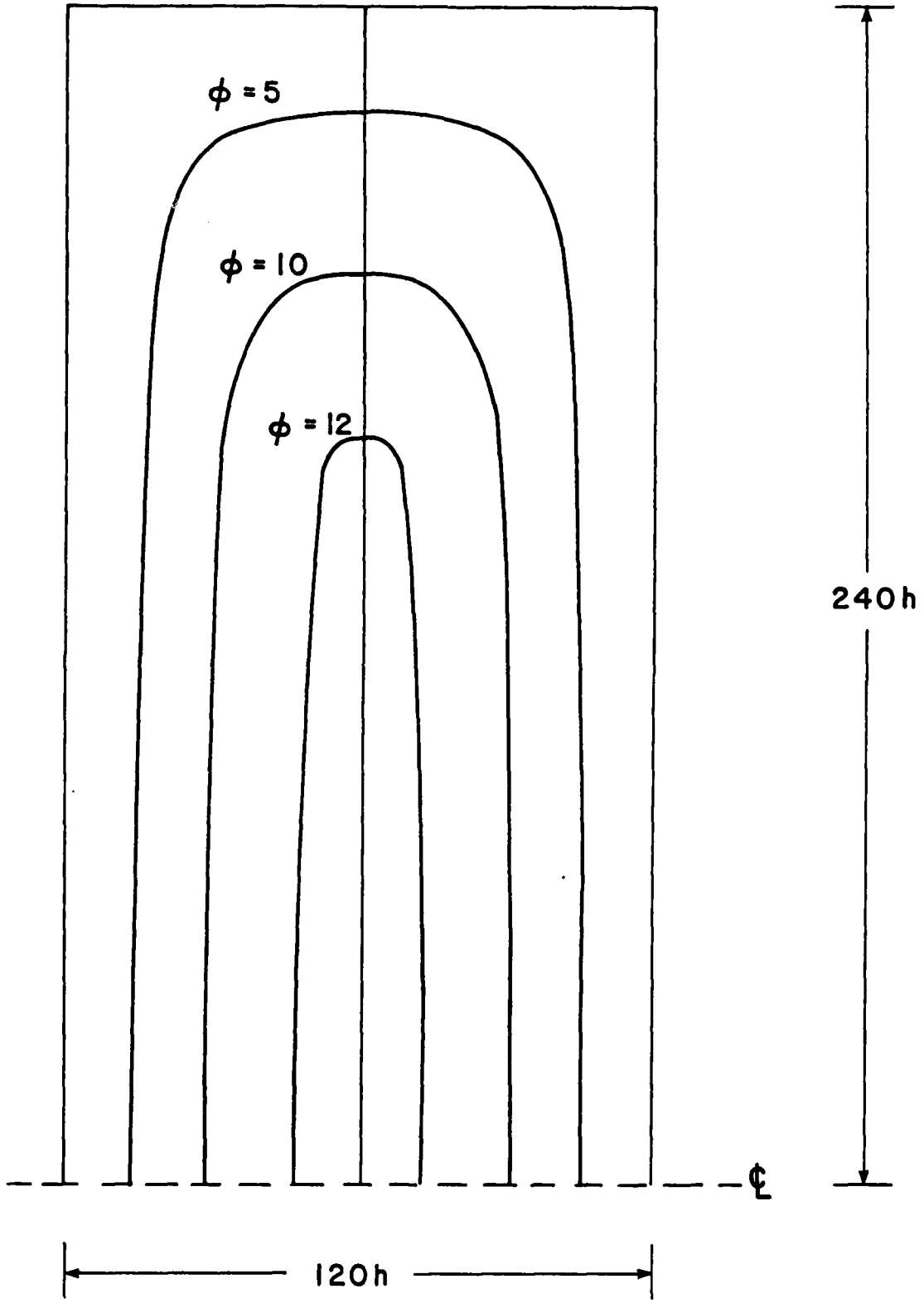

Figure V-17. Stream Function Contours for a Long Rectangular Plate Excited by a Harmonic Uniform Field (R = 0.0012).

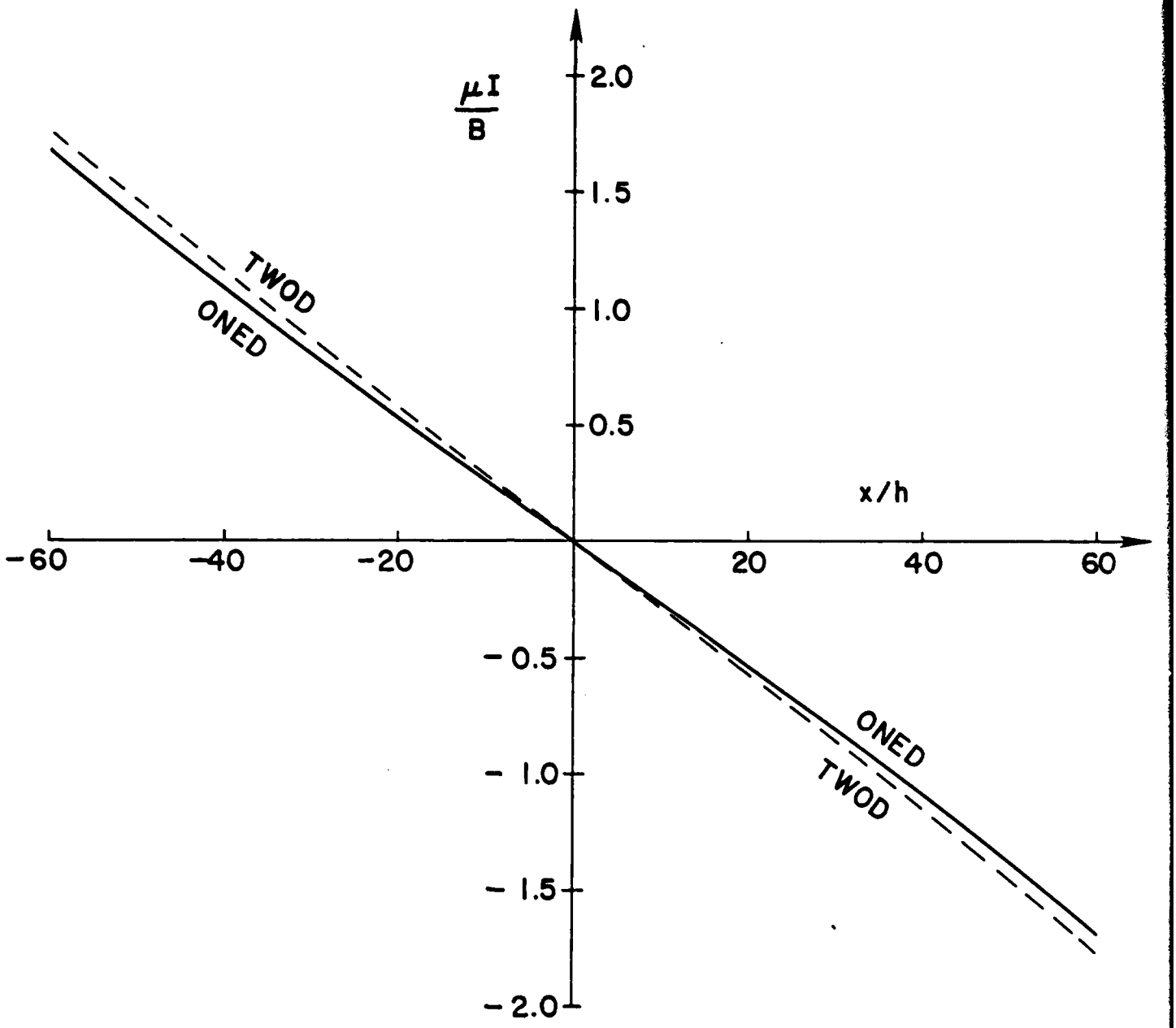

Figure V-18. Comparison of One- and Two-Dimensional Solutions of Currents Induced Across the Middle of a Long Rectangular Plate by a Harmonic Uniform Field (R = 0.03).

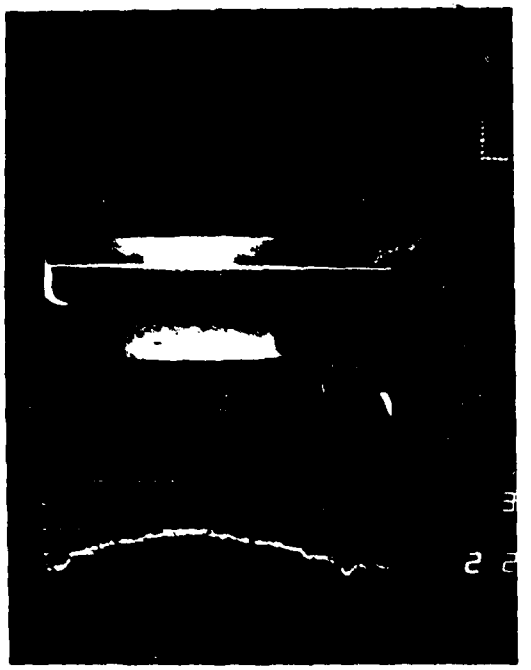

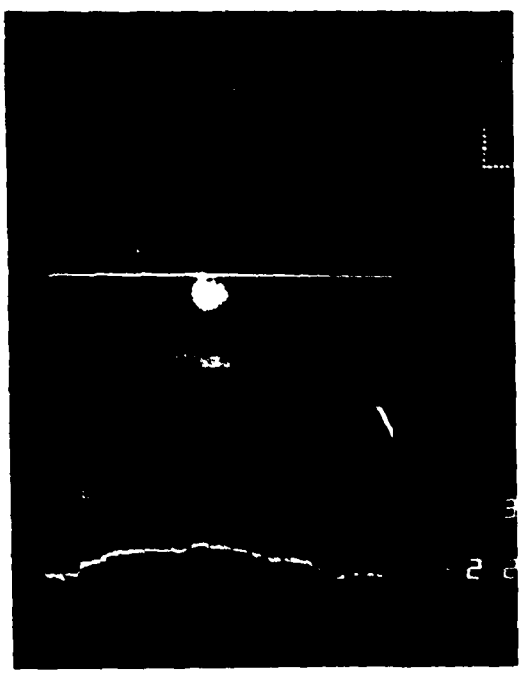

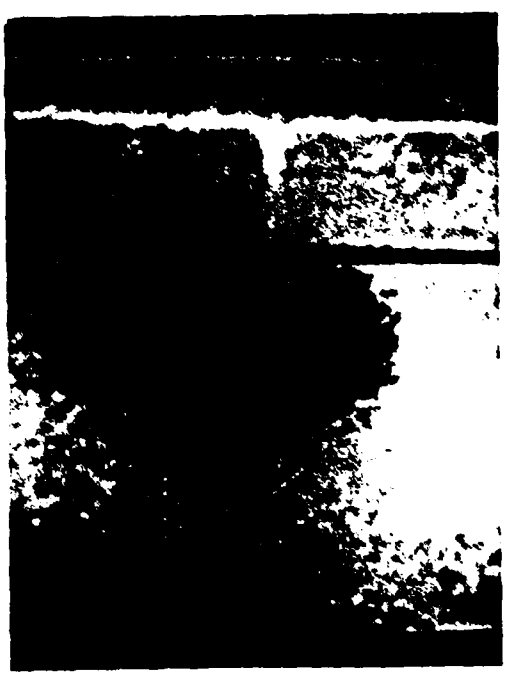

Figure V-10. Infrared Thermogram Showing Hot Spots Due to Eddy Current Flow
upper) plate without a crack.
lower left) hot spot due to flow around a crack.
lower right) color quantized hot spot at top of crack (magnified).

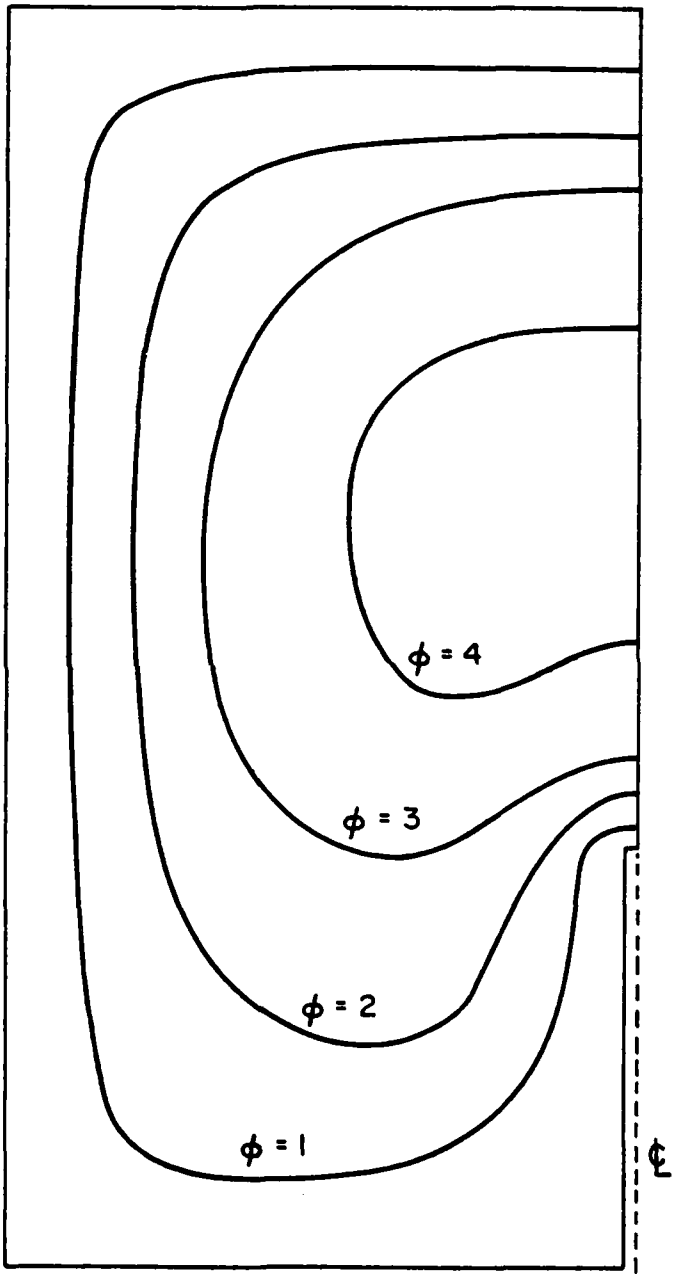

Figure V-20. Stream Function Contours for a Notched Plate Excited by a Harmonic Uniform Field (Notchwidth = 2h, R = 0.001).

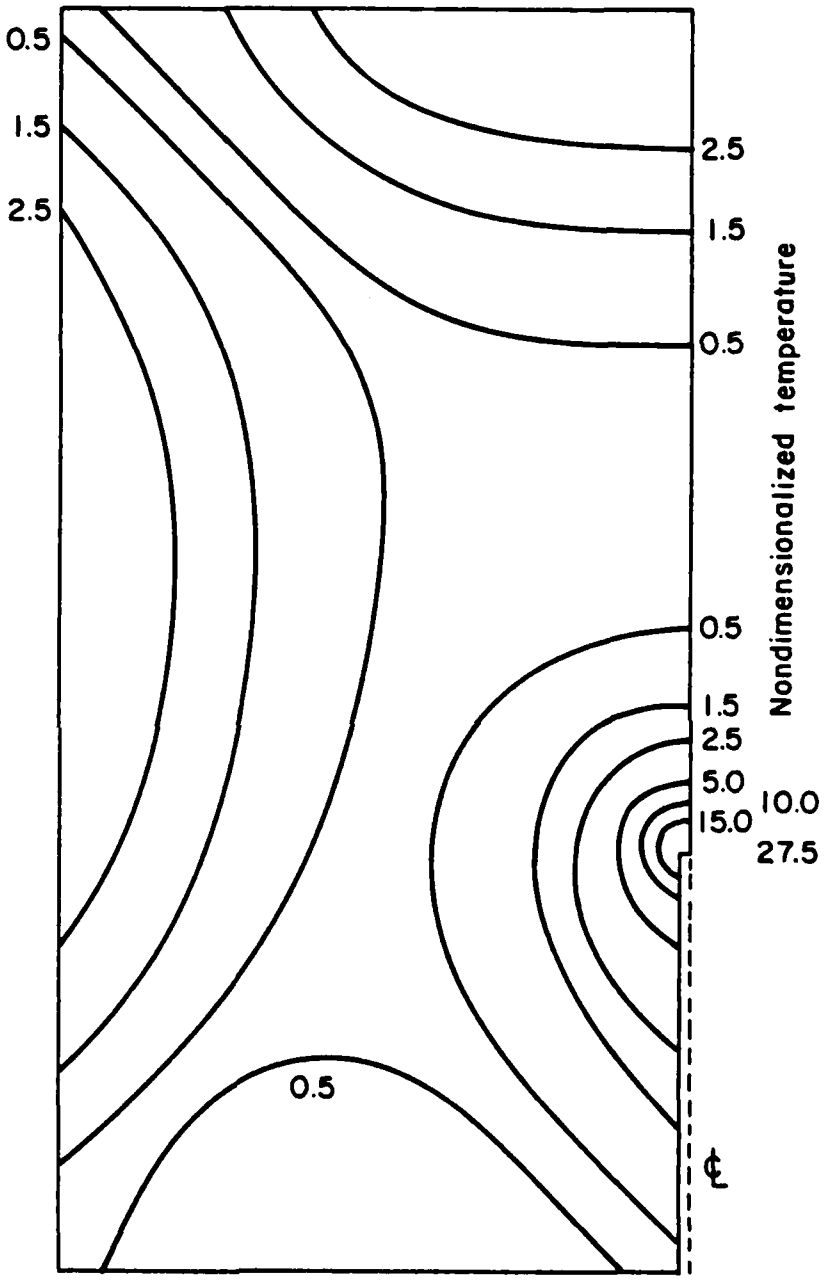

Figure V-21. Isotherms for a Notched Plate Excited by a Harmonic Uniform Field (Notchwidth = 2h, R = 0.001).

VI. CONCLUSIONS

This technical report describes the accomplishments of the first year of a research project directed toward developing numerical methods for the coupled analysis of forces, currents, and stresses in thin elastic structures exposed to time-dependent magnetic fields. A stream function for the induced eddy currents is used to reduce the three-dimensional electromagnetic problem to an integro-differential equation in the two-dimensional surface of the sheet conductor. Although formulations are presented herein for both flat and cylindrically curved conductor sheets, to date the research has focused on the response of flat plates to steady state harmonic and pulsed magnetic fields.

Finite element codes for one- and two-dimensional flat plates have been developed which can calculate the induced current and magnetic fields in the plates, the magnetic pressure distribution on the plates, and the temperature distributions in the plates due to Joule heating. The eddy current calculations include the nonlocal or self-field effects. These programs have been verified by comparison to experimental results and to known analytical solutions.

The programs have been applied to a number of configurations. The results of these analyses give rise to the following conclusions:

1. The numerical method based on the stream function method produces results in agreement with experimental observations and analytical solutions. The success of this method is encouraging because the reduced dimensionality promises significantly greater efficiency than methods based on a full three-dimensional approach. In this sense, the stream function method is analogous to the boundary integral equation method (boundary element method). However, when nonlocal effects are taken into account the algebraic finite element equations become full rather than banded, and this increases the computational cost. This can be ameliorated and a degree of bandedness restored by a proper modi-

fication of the nonlocal integrals to account for the rapid decrease of the self-field effect with increasing distance between sources and field points.

2. For medium to high magnetic Reynolds numbers, the contributions of the self-field effect yield significantly different eddy currents than those predicted by a purely local solution. Most previous work in eddy current prediction and magnetomechanics has neglected this effect. Moreover, for a harmonic field, the nonlocal or self-fields effects must be taken into account to obtain the time-averaged forces on the conductor.

3. The techniques and programs that have been developed will have applications to a number of practical problems. One such application illustrated in this report is the use of induced eddy currents for the nondestructive testing (NDT) for cracks and flaws in sheet-like conductors such as plates and shells. The programs can be used to design and calibrate eddy current probe NDT devices and to develop a catalog of thermograms for various flaws. Another possible application is to geomagnetic prospecting, in which very large induction coils on the surface of the earth might be used to detect the presence, location, and orientation of seams of conducting ores. The programs could be used to simulate this process and thereby play a role in the interpretation of prospecting data.

The present computer programs can be used to predict the dynamic forces on flat plates when the motion of the plate is small. The immediate task of future research is to extend this to large deformations of the conductors where true coupling of the magnetic and mechanical behavior occurs. In addition, it is planned to extend this work to curved conducting surfaces such as cylindrical, toroidal, and other shell configurations. Finally, applications to nondestructive testing are being explored further.

REFERENCES

Cited References

1. T.J. Doyle, "Superconductive Propulsion Motor," (D.W. Taylor Naval Ship R & D Center), Mechanical Engineering, Jan. 1977, pp. 48-53.

2. B.B. Schwartz, Foner, S., "Large-Scale Applications of Superconductivity," Physics Today, July 1977, pp. 34-43.

3. T.E. Alves, "Refining the Magnetic Forming Capability," Final Report, Naval Ordnance Station, Louisville, Kentucky, Report No. MT-008, April 1972.

4. T.E. Alves, "Electromagnetic Swaging: A Case History," Report from Naval Ordnance Station, Louisville, Kentucky, 1973.

5. S.T. Smith, "Vacuum Breakdown," Research Report, Naval Research Laboratory.

6. Moon, F.C. and Swanson, C., Experiments on Buckling and Vibration of Superconducting Coils, ASME Paper No. 77-WA/APM-28, J. Applied Mechanics, Dec. 1977.

7. Moon, F.C. and Swanson, C., Vibration and Stability of a Set of Superconducting Tourdal Magnets, J. Applied Physics, Vol. 47, pp. 914-919.

8. Oden, J.T. and Kelly, B.E., "Finite Element Formulation of General Electro-thermoelasticity Problems," Int. J. Num. Methods Engng., Vol. 3, pp. 161-179, 1971.

9. Miya, K., An, S., Ando, Y., Ohta, M. and Suzuki, Y., "Application of Finite Element Method to Electro-Magneto-Mechanical Dynamics of Superconducting Magnet Coil and Vacuum Vessel," Proc. 6th Symp. of Engineering Problems of of Fusion Research, Nov. 1975, Publ. IEEE, N.Y., 1976, pp. 927-934.

10. Becker, E.B. and Pillsbury, R.D., "Finite Element Analysis of Coupled Electric, Magnetic, and Dynamic Problems," Formulation and Computational Algorithms in Finite Element Analysis, K.J. Bathe, et al., editors, MIT Press, 1977, pp. 1059-1083.

11. Moon, F.C., "Problems in Magneto-Solid Mechanics," Mechanics Today, Nemat-Nasser, S., (Ed.), American Academy of Mechanics, Nov. 1977.

12. Pao, Y.H. and Hutter, K., "Electrodynamics for Moving Elastic Solids and Viscous Fluids," Proc. IEEE, Vol. 63, No. 7, p. 1011, July 1975.

13. Jackson, J.D., Classical Electrodynamics, John Wiley and Sons, N.Y., 1962.

14. Trowbridge, C.W., "Application of Integral Equation Methods for the Numerical Solution of Magnetostatic and Eddy Current Problems," Rep. No. RL-76-071, CAG/76-10, Rutherford Laboratory, June 1976.

15. Silvester, P. and Popovic, B.D., "The Integral Equations of Superconductive Levitation Systems," Digests of the Intermag. Conf., Int. Magnetics Conf. IEEE, Toronto, Canada, May 1974, p. 19.9.

16. Carpenter, K.H., and Yeh, H.T., "Papers on Eddy Current Calculations," ORNL/TM-5652, Oak Ridge National Laboratory, Dec. 1976.

17. De Mey, G.G., "A Method for Calculating Eddy Currents in Plates of Arbitrary Geometry," Archiv für Elektrotechnik 56 (1974), pp. 137-140, Springer-Verlag, 1974.

18. Sylvester, P., Wong, S.K., and Buke, P.E., "Modal Theory of Ski Effect in Single and Multiple Turn Coils," IEEE Trans on PAS, Vol. PAS-91, pp. 29-34, 1972.

19. Forrestal, M.J., "The Response of Ring Structures to Impulse Loads", Simulation Research Department, Sandia Laboratories, Albuquerque, N.M., November 1976.

20. Kameari, A., and Suzuki, Y., "Eddy Current Analysis by the Finite Element Circuit Method", Proceedings of the 7th Symposium on Engineering Problems of Fusion Research, Knoxville, TN, 1977, pp. 1386-1392.

APPENDIX A

Description of Experimental Apparatus

Description of UTI Infrared Scanner

Commercially available infrared detectors include point sensing, line, and two-dimensional or plane scanners. Two different commercial plane scanners have been used over the history of this research program, though for the reported phase of the study only the UTI Scanner was used.

The scanner consists of three main subsystems: (1) the detector, (2) the continuous grey coding of temperatures on a black and white monitor, and (3) a color coding and color display monitor. The scanner used was manufactured by UTI Corp. of Sunnydale, California based on an earlier design called Spectrotherm 2000, by another company. The detector is a mercury cadmium telluride (*HgCdTe*) crystal maintained at 78°K by liquid nitrogen. HgCdTe is a photoconductive element sensitive to infrared radiation in the 2-12 μm wavelength range. Radiation from different points in the field are focused on the crystal by two rotating mirrors for both horizontal and vertical scans.

The sensitivity of this unit is as low as 0.2°C. The output from the crystal detector is used to produce a variable grey spot on a cathode ray display tube. White to black grey tones can be used for hot to cold or visa versa. An isotherm option is available as well as a graphics temperature display. One horizontal scan of temperatures is graphed below the two-dimensional grey image of the temperature field.

The two-dimensional grey infrared picture has 525 raster lines and 600 elements per line on a 7.6 cm x 7.6 cm screen. The field can be focused from 10 cm to 6 meters. The depth of field is 15 cm at a distance of 80 cm.

The scan and graphic temperature display takes 2 seconds, though on a newer model a one-second option is available.

The electronic data can be stored electronically indefinitely so that pictures can be taken of the display tube. Also a zoom capability can be used to magnify and examine only part of the scanned field.

Finally the data can be color quantized in a separate unit. The UTI uses a Sony Trinitron (trade name) 12.7 x 19.7 cm display screen and ten colors. Each color represents a temperature interval. The resulting display is a beautiful color set of isotherms.

The AGA Corp. also manufactures a two-dimensional field scanner system. The scan time is shorter (16 per second) but the image is coarser (210 horizontal lines, 140 elements per line) and no storage of data was possible. This unit was used in earlier research, however, with some success.

Specimen Preparation

The ammount of radiation transmitted to the detector depends not only on the temperature of the transmitting object but on its emissivity. To avoid spurious data due to differences in emissivity the conductors were sprayed with a high emissivity, black coating. Two brands used were NEXTEL brand Suede coating (3101 series) and 3M Velvet Coating-Optical Black. These coatings also decreased spurious infrared reflections from other objects.

Search Coil Apparatus

The infrared data was compared with experimentally measured eddy currents by using a differential search coil. It is known from electromagnetics that the jump in tangential magnetic field ocross a thin conductor is directly proportional to the current in the conductor. To measure the tangential magnetic field at the surface of the plate, two small multi-turn coils were wound and aligned with their axes parallel with the plate. The induced currents then

generate time-dependent magnetic fields which can be detected by these coils. Since the output voltage is proportional to the change in magnetic field, a passive R-C integrating circuit was used in series with the coils.

The coils were connected to cancel voltages. Thus the primary field of the induction coil would produce almost zero voltage in the differential coils. (Small errors due to the finite separation of the coils and the inhomogeneity of the induction coil field can occur). The resulting voltage is almost entirely due to the field of the eddy currents.

APPENDIX B

Personnel Engaged in the Research

The following Cornell University personnel have been engaged in the research during part or all of the first year of the project:

John F. Abel, Associate Professor of Structural Engineering, Co-Principal Investigator

Frances C. Moon, Associate Professor of Theoretical and Applied Mechanics, Co-Principal Investigator

Kuan-Ya Yuan, Graduate Student in the Department of Structural Engineering, Graduate Research Assistant

Kosei Hara, Graduate Student in the Department of Theoretical and Applied Mechanics, Graduate Research Assistant

Timothy Bond, Electrical Engineer on the Technical Staff of the Department of Theoretical and Applied Mechanics, Laboratory Assistant

APPENDIX C

Communication of Technical Results

The following technical papers and oral presentations at scientific and engineering meetings have emerged from this research to date:

Technical Paper

K.Y. Yuan, F.C. Moon, and J.F. Abel, "Magnetic Forces in Plates Using Finite Elements", Proceedings, Third Engineering Mechanics Division Specialty Conference, ASCE, New York, 1979, pp. 730-733.

Oral Presentations

F.C. Moon, "Infrared Measurements of Induced Eddy Currents in Sheet Conductors", Joint INTERMAG MMM Conference, New York, July 18, 1979.

K.Y. Yuan, "Magnetic Forces in Plates Using Finite Elements", Third ASCE/EMD Specialty Conference, University of Texas at Austin, September 19, 1979.

474:NP:716:lab
78u474-619

DISTRIBUTION LIST

Part 1 - Government
Administrative and Liaison Activities

Office of Naval Research
Department of the Navy
Arlington, Virginia 22217
Attn: Code 474 (2)
Code 471
Code 200

Director
Office of Naval Research
Branch Office
666 Summer Street
Boston, Massachusetts 02210

Director
Office of Naval Research
Branch Office
536 South Clark Street
Chicago, Illinois 60605

Director
Office of Naval Research
New York Area Office
715 Broadway - 5th Floor
New York, New York 10003

Director
Office of Naval Research
Branch Office
1030 East Green Street
Pasadena, California 91106

Naval Research Laboratory (6)
Code 2627
Washington, D.C. 20375

Defense Documentation Center (12)
Cameron Station
Alexandria, Virginia 22314

Navy

Undersea Explosion Research Division
Naval Ship Research and Development
Center
Norfolk Naval Shipyard
Portsmouth, Virginia 23709
Attn: Dr. E. Palmer, Code 177

Navy (Con't.)

Naval Research Laboratory
Washington, D.C. 20375
Attn: Code 8400
8410
8430
8440
6300
6390
6380

David W. Taylor Naval Ship Research
and Development Center
Annapolis, Maryland 21402
Attn: Code 2740
28
281

Naval Weapons Center
China Lake, California 93555
Attn: Code 4062
4520

Commanding Officer
Naval Civil Engineering Laboratory
Code L31
Port Hueneme, California 93041

Naval Surface Weapons Center
White Oak
Silver Spring, Maryland 20910
Attn: Code R-10
G-402
K-82

Technical Director
Naval Ocean Systems Center
San Diego, California 92152

Supervisor of Shipbuilding
U.S. Navy
Newport News, Virginia 23607

Navy Underwater Sound
Reference Division
Naval Research Laboratory
P.O. Box 8337
Orlando, Florida 32806

474:NP:716:lab
78u474-619

Navy (Con't.)

Chief of Naval Operations
Department of the Navy
Washington, D.C. 20350
Attn: Code OP-098

Strategic Systems Project Office
Department of the Navy
Washington, D.C. 20376
Attn: NSP-200

Naval Air Systems Command
Department of the Navy
Washington, D.C. 20361
Attn: Code 5302 (Aerospace and Structures)
604 (Technical Library)
320B (Structures)

Naval Air Development Center
Warminster, Pennsylvania 18974
Attn: Aerospace Mechanics
Code 606

U.S. Naval Academy
Engineering Department
Annapolis, Maryland 21402

Naval Facilities Engineering Command
200 Stovall Street
Alexandria, Virginia 22332
Attn: Code 03 (Research and Development)
04B
045
14114 (Technical Library)

Naval Sea Systems Command
Department of the Navy
Washington, D.C. 20362
Attn: Code 05H
312
322
323
05R
32R

Navy (Con't.)

Commander and Director
David W. Taylor Naval Ship
Research and Development Center
Bethesda, Maryland 20084
Attn: Code 042
17
172
173
174
1800
1844
012.2
1900
1901
1945
1960
1962

Naval Underwater Systems Center
Newport, Rhode Island 02840
Attn: Dr. R. Trainor

Naval Surface Weapons Center
Dahlgren Laboratory
Dahlgren, Virginia 22448
Attn: Code G04
G20

Technical Director
Mare Island Naval Shipyard
Vallejo, California 94592

U.S. Naval Postgraduate School
Library
Code 0384
Monterey, California 93940

Webb Institute of Naval Architecture
Attn: Librarian
Crescent Beach Road, Glen Cove
Long Island, New York 11542

Army

Commanding Officer (2)
U.S. Army Research Office
P.O. Box 12211
Research Triangle Park, NC 27709
Attn: Mr. J. J. Murray, CRD-AA-IP

474:NP:716:lab
78u474-619

Army (Con't.)

Watervliet Arsenal
MAGGS Research Center
Watervliet, New York 12189
Attn: Director of Research

U.S. Army Materials and Mechanics
Research Center
Watertown, Massachusetts 02172
Attn: Dr. R. Shea, DRXMR-T

U.S. Army Missile Research and
Development Center
Redstone Scientific Information
Center
Chief, Document Section
Redstone Arsenal, Alabama 35809

Army Research and Development
Center
Fort Belvoir, Virginia 22060

NASA

National Aeronautics and Space
Administration
Structures Research Division
Langley Research Center
Langley Station
Hampton, Virginia 23365

National Aeronautics and Space
Administration
Associate Administrator for Advanced
Research and Technology
Washington, D.C. 20546

Air Force

Wright-Patterson Air Force Base
Dayton, Ohio 45433
Attn: AFFDL (FB)
(FBR)
(FBE)
(FBS)
AFML (MBM)

Air Force (Con't.)

Chief Applied Mechanics Group
U.S. Air Force Institute of Technology
Wright-Patterson Air Force Base
Dayton, Ohio 45433

Chief, Civil Engineering Branch
WLRC, Research Division
Air Force Weapons Laboratory
Kirtland Air Force Base
Albuquerque, New Mexico 87117

Air Force Office of Scientific Researc
Bolling Air Force Base
Washington, D.C. 20332
Attn: Mechanics Division

Department of the Air Force
Air University Library
Maxwell Air Force Base
Montgomery, Alabama 36112

Other Government Activities

Commandant
Chief, Testing and Development Divisic
U.S. Coast Guard
1300 E Street, NW.
Washington, D.C. 20226

Technical Director
Marine Corps Development
and Education Command
Quantico, Virginia 22134

Director Defense Research
and Engineering
Technical Library
Room 3C128
The Pentagon
Washington, D.C. 20301

474:NP:716:lab
78u474-619

Other Government Activities (Con't)

Dr. M. Gaus
National Science Foundation
Environmental Research Division
Washington, D.C. 20550

Library of Congress
Science and Technology Division
Washington, D.C. 20540

Director
Defense Nuclear Agency
Washington, D.C. 20305
Attn: SPSS

Mr. Jerome Persh
Staff Specialist for Materials
and Structures
OUSDR&E, The Pentagon
Room 3D1089
Washington, D.C. 20301

Chief, Airframe and Equipment Branch
FS-120
Office of Flight Standards
Federal Aviation Agency
Washington, D.C. 20553

National Academy of Sciences
National Research Council
Ship Hull Research Committee
2101 Constitution Avenue
Washington, D.C. 20418
Attn: Mr. A. R. Lytle

National Science Foundation
Engineering Mechanics Section
Division of Engineering
Washington, D.C. 20550

Picatinny Arsenal
Plastics Technical Evaluation Center
Attn: Technical Information Section
Dover, New Jersey 07801

Maritime Administration
Office of Maritime Technology
14th and Constitution Avenue, NW.
Washington, D.C. 20230

PART 2 - Contractors and Other Technical Collaborators

Universities

Dr. J. Tinsley Oden
University of Texas at Austin
345 Engineering Science Building
Austin, Texas 78712

Professor Julius Miklowitz
California Institute of Technology
Division of Engineering
and Applied Sciences
Pasadena, California 91109

Dr. Harold Liebowitz, Dean
School of Engineering and
Applied Science
George Washington University
Washington, D.C. 20052

Professor Eli Sternberg
California Institute of Technology
Division of Engineering and
Applied Sciences
Pasadena, California 91109

Professor Paul M. Naghdi
University of California
Department of Mechanical Engineering
Berkeley, California 94720

Professor A. J. Durelli
Oakland University
School of Engineering
Rochester, Missouri 48063

Professor F. L. DiMaggio
Columbia University
Department of Civil Engineering
New York, New York 10027

Professor Norman Jones
The University of Liverpool
Department of Mechanical Engineering
P. O. Box 147
Brownlow Hill
Liverpool L69 3BX
England

Professor E. J. Skudrzyk
Pennsylvania State University
Applied Research Laboratory
Department of Physics
State College, Pennsylvania 16801

Universities (Con't.)

Professor J. Klosner
Polytechnic Institute of New York
Department of Mechanical and
Aerospace Engineering
333 Jay Street
Brooklyn, New York 11201

Professor R. A. Schapery
Texas A&M University
Department of Civil Engineering
College Station, Texas 77843

Professor Walter D. Pilkey
University of Virginia
Research Laboratories for the
Engineering Sciences and
Applied Sciences
Charlottesville, Virginia 22901

Professor K. D. Willmert
Clarkson College of Technology
Department of Mechanical Engineering
Potsdam, New York 13676

Dr. Walter E. Haisler
Texas A&M University
Aerospace Engineering Department
College Station, Texas 77843

Dr. Hussein A. Kamel
University of Arizona
Department of Aerospace and
Mechanical Engineering
Tucson, Arizona 85721

Dr. S. J. Fenves
Carnegie-Mellon University
Department of Civil Engineering
Schenley Park
Pittsburgh, Pennsylvania 15213

Dr. Ronald L. Huston
Department of Engineering Analysis
University of Cincinnati
Cincinnati, Ohio 45221

Universities (Con't)

Professor G. C. M. Sih
Lehigh University
Institute of Fracture and
Solid Mechanics
Bethlehem, Pennsylvania 18015

Professor Albert S. Kobayashi
University of Washington
Department of Mechanical Engineering
Seattle, Washington 98105

Professor Daniel Frederick
Virginia Polytechnic Institute and
State University
Department of Engineering Mechanics
Blacksburg, Virginia 24061

Professor A. C. Eringen
Princeton University
Department of Aerospace and
Mechanical Sciences
Princeton, New Jersey 08540

Professor E. H. Lee
Stanford University
Division of Engineering Mechanics
Stanford, California 94305

Professor Albert I. King
Wayne State University
Biomechanics Research Center
Detroit, Michigan 48202

Dr. V. R. Hodgson
Wayne State University
School of Medicine
Detroit, Michigan 48202

Dean B. A. Boley
Northwestern University
Department of Civil Engineering
Evanston, Illinois 60201

474:NP:716:lab
78u474-619

Universities (Con't)

Professor P. G. Hodge, Jr.
University of Minnesota
Department of Aerospace Engineering
and Mechanics
Minneapolis, Minnesota 55455

Dr. D. C. Drucker
University of Illinois
Dean of Engineering
Urbana, Illinois 61801

Professor N. M. Newmark
University of Illinois
Department of Civil Engineering
Urbana, Illinois 61803

Professor E. Reissner
University of California, San Diego
Department of Applied Mechanics
La Jolla, California 92037

Professor William A. Nash
University of Massachusetts
Department of Mechanics and
Aerospace Engineering
Amherst, Massachusetts 01002

Professor G. Herrmann
Stanford University
Department of Applied Mechanics
Stanford, California 94305

Professor J. D. Achenbach
Northwest University
Department of Civil Engineering
Evanston, Illinois 60201

Professor S. B. Dong
University of California
Department of Mechanics
Los Angeles, California 90024

Professor Burt Paul
University of Pennsylvania
Towne School of Civil and
Mechanical Engineering
Philadelphia, Pennsylvania 19104

Universities (Con't)

Professor H. W. Liu
Syracuse University
Department of Chemical Engineering
and Metallurgy
Syracuse, New York 13210

Professor S. Bodner
Technion R&D Foundation
Haifa, Israel

Professor Werner Goldsmith
University of California
Department of Mechanical Engineering
Berkeley, California 94720

Professor R. S. Rivlin
Lehigh University
Center for the Application
of Mathematics
Bethlehem, Pennsylvania 18015

Professor F. A. Cozzarelli
State University of New York at
Buffalo
Division of Interdisciplinary Studies
Karr Parker Engineering Building
Chemistry Road
Buffalo, New York 14214

Professor Joseph L. Rose
Drexel University
Department of Mechanical Engineering
and Mechanics
Philadelphia, Pennsylvania 19104

Professor B. K. Donaldson
University of Maryland
Aerospace Engineering Department
College Park, Maryland 20742

Professor Joseph A. Clark
Catholic University of America
Department of Mechanical Engineering
Washington, D.C. 20064

474:NP:716:lab
78u474-619

Universities (Con't)

Dr. Samuel B. Batdorf
University of California
School of Engineering
and Applied Science
Los Angeles, California 90024

Professor Isaac Fried
Boston University
Department of Mathematics
Boston, Massachusetts 02215

Professor E. Krempl
Rensselaer Polytechnic Institute
Division of Engineering
Engineering Mechanics
Troy, New York 12181

Dr. Jack R. Vinson
University of Delaware
Department of Mechanical and Aerospace
Engineering and the Center for
Composite Materials
Newark, Delaware 19711

Dr. J. Duffy
Brown University
Division of Engineering
Providence, Rhode Island 02912

Dr. J. L. Swedlow
Carnegie-Mellon University
Department of Mechanical Engineering
Pittsburgh, Pennsylvania 15213

Dr. V. K. Varadan
Ohio State University Research Foundation
Department of Engineering Mechanics
Columbus, Ohio 43210

Dr. Z. Hashin
University of Pennsylvania
Department of Metallurgy and
Materials Science
College of Engineering and
Applied Science
Philadelphia, Pennsylvania 19104

Universities (Con't)

Dr. Jackson C. S. Yang
University of Maryland
Department of Mechanical Engineering
College Park, Maryland 20742

Professor T. Y. Chang
University of Akron
Department of Civil Engineering
Akron, Ohio 44325

Professor Charles W. Bert
University of Oklahoma
School of Aerospace, Mechanical,
and Nuclear Engineering
Norman, Oklahoma 73019

Professor Satya N. Atluri
Georgia Institute of Technology
School of Engineering and
Mechanics
Atlanta, Georgia 30332

Professor Graham F. Carey
University of Texas at Austin
Department of Aerospace Engineering
and Engineering Mechanics
Austin, Texas 78712

Dr. S. S. Wang
University of Illinois
Department of Theoretical and
Applied Mechanics
Urbana, Illinois 61801

Industry and Research Institutes

Dr. Norman Hobbs
Kaman AviDyne
Division of Kaman
Sciences Corporation
Burlington, Massachusetts 01803

Argonne National Laboratory
Library Services Department
9700 South Cass Avenue
Argonne, Illinois 60440

474:NP:716:lab
78u474-619

Industry and Research Institutes (Con't)

Dr. M. C. Junger
Cambridge Acoustical Associates
54 Rindge Avenue Extension
Cambridge, Massachusetts 02140

Dr. V. Godino
General Dynamics Corporation
Electric Boat Division
Groton, Connecticut 06340

Dr. J. E. Greenspon
J. G. Engineering Research Associates
3831 Menlo Drive
Baltimore, Maryland 21215

Newport News Shipbuilding and
Dry Dock Company
Library
Newport News, Virginia 23607

Dr. W. F. Bozich
McDonnell Douglas Corporation
5301 Bolsa Avenue
Huntington Beach, California 92647

Dr. H. N. Abramson
Southwest Research Institute
8500 Culebra Road
San Antonio, Texas 78284

Dr. R. C. DeHart
Southwest Research Institute
8500 Culebra Road
San Antonio, Texas 78284

Dr. M. L. Baron
Weidlinger Associates
110 East 59th Street
New York, New York 10022

Dr. T. L. Geers
Lockheed Missiles and Space Company
3251 Hanover Street
Palo Alto, California 94304

Mr. William Caywood
Applied Physics Laboratory
Johns Hopkins Road
Laurel, Maryland 20810

Industry and Research Institutes (Con't)

Dr. Robert E. Dunham
Pacifica Technology
P.O. Box 148
Del Mar, California 92014

Dr. M. F. Kanninen
Battelle Columbus Laboratories
505 King Avenue
Columbus, Ohio 43201

Dr. A. A. Hochrein
Daedalean Associates, Inc.
Springlake Research Road
15110 Frederick Road
Woodbine, Maryland 21797

Dr. James W. Jones
Swanson Service Corporation
P.O. Box 5415
Huntington Beach, California 92646

Dr. Robert E. Nickell
Applied Science and Technology
3344 North Torrey Pines Court
Suite 220
La Jolla, California 92037

Dr. Kevin Thomas
Westinghouse Electric Corp.
Advanced Reactors Division
P. O. Box 158
Madison, Pennsylvania 15663